Atmospheric Water Generation

A Major Qualifying Project Report:

Submitted to the Faculty

of

WORCESTER POLYTECHNIC INSTITUTE

in partial fulfillment of the requirements for the

Degree of Bachelor of Science

by

Christopher Bolsinger

Spencer Ralphs

April 25, 2019

Approved:

Dr. Jamal S. Yagoobi, Advisor

Abstract

Affordable access to potable water is a global issue, as approximately 844 million people around the world lack access to clean water. Atmospheric water generation can address this issue by generating potable water from the water vapor present in air. One technology to be utilized for atmospheric water generation is the vapor compression cycle (VCC), which generates water from ambient air by cycling a refrigerant to create a cold surface on which water vapor will condense. The parameters for condensation are dependent upon environmental constraints, including temperature and humidity of the ambient air. The scope of this project is to design and build a prototype VCC capable of delivering 500cc of liquid water from ambient air per hour. To do this, the system was first simulated using the relevant thermodynamic and heat transfer phenomena in the VCC to determine the design parameters. The simulation results dictated the purchasing of various components and assembling of hardware to achieve the aforementioned goal of 500cc/hour as a proof of concept for further future research into adaptation for large scale ecological applications, such as hydroponic greenhouses. With successful water generation in low humidity ambient Worcester conditions, the VCC will be extremely efficacious in supplying potable water to a community when integrated in a constantly humid hydroponic greenhouse.

Acknowledgments

We would like to thank the Mechanical Engineering department at WPI for providing the necessary resources and laboratory space for completing this project. We would also like to thank our advisor, Dr. Jamal Yagoobi, for providing consistent guidance and insight throughout the project. Finally, we would like to thank PhD students Alexander Castaneda, Nathaniel O'Connor, and Livia Motz for being instrumental in the success of the project through their assistance in design, fabrication, and testing of the experimental setup.

Table of Contents

Contents

Abstract 1

Acknowledgments 2

Table of Contents 3

List of Figures 5

List of Tables 6

Nomenclature 7

Executive Summary 8

Introduction 9

Available Technology 11

Vapor Compression Cycles (VCC) 11

Competing Technologies 13

Vapor Absorption Cycle (VAC) 13

Thermoacoustic Cooling (TAC) 14

Thermoelectric Cooling (TEC) 14

Desiccation for Water Generation 15

Gas Separation Membranes 16

Emerging Technology 17

Summary of VCC Governing Equations 19

Refrigerant Selection & Justification 21

Assumptions and Parameters Assumed 21

Thermodynamic States and Operating Pressures: 21

Heat Exchanger Material Selection: 22

Ambient Assumptions: 23

Nominal Assumptions & State Points 24

Design 24

Results 26

Design Results Discussion 27

Ethical Considerations 27

Instrumentation & Assembly 28

Heat Exchanger Fabrication 29

Brazing....30
Leak Testing....35
Compressor Wiring....36
Experimental Setup....38
Experimental Results and Analysis....40
Cost Analysis....46
Conclusions & Recommendations....48
References....49
Appendix 1: R-1234ze Pressure-Enthalpy Data....51
Appendix 2: R-1234ze Pressure-Temperature Data....51
Appendix 3: R-134a Comparison....52
Appendix 4: Evaporator Length Script....52
Appendix 5: Condenser Length Script....53
Appendix 6: Detailed P&ID....53
Appendix 7: Refrigerant Weight Calculations....54
Appendix 8: LabView Front Panel....54
Appendix 9: LabView Block Diagram....55

List of Figures

Figure 1: Schematic of holistic project integration and eventual application combining food, energy, and water using the vapor compression cycle. 10
Figure 2: T-s diagram for ideal VCC 12
Figure 3: Schematic of an ideal VCC 12
Figure 4: Thermal expansion valve diagram 12
Figure 5: Vapor absorption cycle schematic 13
Figure 6: Thermoacoustic cooling schematic 14
Figure 7: Thermoelectric cooling schematic 15
Figure 8: Desiccation system schematic 16
Figure 9: Gas separation system with vacuum as driving force 17
Figure 10: MOF schematic 18
Figure 11: Performance data sheet 22
Figure 12: P&ID of experimental VCC 29
Figure 13: Tube bending device 30
Figure 14: Evaporator tubing 30
Figure 15: Condenser tubing 30
Figure 16: Paste flux application 31
Figure 17: Tubing with paste flux 31
Figure 18: Brazing application 32
Figure 19: Brazing application cont. 32
Figure 20: Evaporator with instruments added 33
Figure 21: Condenser with instruments added 33
Figure 22: Expansion valve 34
Figure 23: Full system assembly (without compressor) 34
Figure 24: Leak testing 35
Figure 25: Leak testing cont. 35
Figure 26: System loop with insulation 36
Figure 27: RSID wiring diagram 37
Figure 28: Wired compressor 37
Figure 29: Fully assembled VCC 38
Figure 30: Cleaning setup 39
Figure 31: Final experimental setup 40
Figure 32: First run pressures 41
Figure 33: First run condenser temperatures 41
Figure 34: Frosted evaporator 42
Figure 35: First run evaporator temperatures 42
Figure 36: Added precision valve 43
Figure 37: Evaporator with layer of condensed water 43
Figure 38: Second run evaporator temperatures 44
Figure 39: Second run condenser temperatures 44
Figure 40: Second run pressures 45
Figure 41: R-1234ze pressure-enthalpy data 51

Figure 42: R-1234ze pressure-temperature data 51
Figure 43: R-134a comparison 52
Figure 44: Evaporator length Matlab script 52
Figure 45: Condenser length Matlab script 53
Figure 46: Detailed P&ID 53
Figure 47: LabView front panel 54
Figure 48: Left side of block diagram 55
Figure 49: Right side of block diagram 56

List of Tables

Table 1: Nomenclature used in Results section 7
Table 2: Technology comparison 17
Table 3: Sustainability and thermodynamic properties of refrigerant options 21
Table 4: Copper tubing size guide (www.supplyhouse.com) 23
Table 5: Copper tubing working pressures 23
Table 6: Nominal assumptions and state points 24
Table 7: Results for Governing Equations 27
Table 8: High side and general use costs 46
Table 9: Low side costs 47
Table 10: Total system cost 47
Table 11: Refrigerant weight calculations 54

Nomenclature

Symbol	Description	Units
A	Surface Area	m^2
D_i	Inside Diameter of Pipe	m
D_o	Outside Diameter of Pipe	m
h_{fg}	Latent Heat	kJ/kg
h_i	Inside Fluid Convective Heat Transfer Coefficient	$W/(m^2\ K)$
h_o	Outside Fluid Convective Heat Transfer Coefficient	$W/(m^2\ K)$
h_1	Refrigerant Enthalpy Entering Compressor	kJ/kg
h_2	Refrigerant Enthalpy Exiting Compressor	kJ/kg
K	Thermal Conductivity of Pipe	$W/(mK)$
k	Constant For Isentropic Conditions	1.4
L	Length of Pipe	m
$\dot{m}$	Mass flow Rate	kg/s
η	Isentropic Efficiency	N/A
P_1	Inlet Pressure to Compressor	K
P_2	Outlet Pressure to Compressor	K
Q	Total Heat Loss/Gain	W
R	Universal Gas Constant	$J/mol\ K$
T_1	Inlet Temperature to Compressor	K
ΔT	Difference in Temperature between flowing refrigerant and ambient air	K
U	Conductance	$W/\ K$
W_c	Compressor Work	kW

Table 1: Nomenclature used in Results section

Executive Summary

Access to clean water is a growing issue throughout the world. Roughly 844 million people, in mostly underdeveloped African nations, do not have clean water. Even larger industrialized nations rely heavily on the use of bottled water, creating unnecessary plastic waste. Common processes of water purification, such as nanofiltration and reverse osmosis desalination, are extremely energy intensive and create waste from the extracted impurities in water. An attractive alternative to deliver clean drinking water is atmospheric water generation. There is an estimated 13 trillion liters of water captured in the air as vapor, providing great potential for clean water generation. The most widespread technique for capturing atmospheric water is to use cooled surfaces to condense the water vapor. It is desired to implement such a system in a hydroponic greenhouse to take advantage of its controlled high humidity level. Many underdeveloped parts of the world already have greenhouses or access to the resources to build one, so the use of atmospheric water generation is extremely attractive. Several refrigeration technologies can perform this function. The vapor compression cycle is the best alternative to generate clean water, given its high efficiency, ability to operate with large work requirements, usage of safe and environmentally friendly refrigerants, and close control of the cycle output. This project investigates the design parameters for a vapor compression cycle used to generate 500 cc of water per hour, including the working fluid, condenser and evaporator surface areas and heat loads, and compressor power.

The working fluid decided upon is R-1234ze, a new HFO refrigerant that was chosen due to its low operating pressures, low global warming potential, and similar performance to the commonly used HFC refrigerant, R-134a. R-1234ze operates between pressures of 179 kPa (1.79 Bar) on the evaporator side and 780 kPa (7.8 Bar) on the condenser side. This results in overall conductance (UA) values for the condenser and evaporator of 21.43 W/K and 34.57 W/K respectively. This was achieved with a calculated condenser length of 0.67 meters and an evaporator length of 0.32 meters resulting in heat extraction of 345.7 W and heat rejection of 460.7 W. The compressor work to achieve these values is 115.6 W. These values dictated system design, component purchasing, fabrication, and assembly.

Utilizing optimization techniques for nonlinear systems of equations, such as the Lagrange multiplier technique, one may arrive at a higher system efficiency, however, due to time constraints, this method was not deployed in this study. This is a point that requires further research and development in order to design and build the most efficacious solution.

Introduction

A growing number of the world's population lack access to clean water. About 844 million people lack access to safe water, a large proportion coming from underdeveloped African countries ("Water Crisis," n.d.). Those with access to water in these countries often have to walk several hours each day to collect clean water. Even developed nations struggle with access to safe water. For example, about 75 percent of Mexico's population drinks packaged water, and in the United States and China, over 10 billion gallons of bottled water are consumed every year as a result of increasing population coupled with climate change and pollution issues (Illsley, 2016). Consequently, the world demand for water treatment products is increasing about seven percent annually ("World Water Treatment," n.d.).

A common process used to generate clean water is desalination, although desalination processes for water treatment are energy intensive and are not economically suitable for areas of the world in need of clean water. Two widespread methods for desalination include membrane filtration and distillation. Reverse osmosis and nanofiltration desalination require pressures up to 1,000 psig as driving forces for the membrane filtration system, while distillation requires an abundant amount of heat to evaporate and condense the water for mineral separation (Cordova, Furukawa, O'Keeffe and Yaghi, 2013). Along with being extremely costly, these processes pose a threat to the environment and result in a waste solution that requires disposal. These water purification methods also require access to a local body of water, which may not be available.

Atmospheric water generation using dehumidification technology is an alternative to high energy desalination systems. These systems could be used to generate potable water in any location with an external power source or renewable energy resources. Dehumidification systems would also be extremely effective when used in greenhouses due to their high humidity levels. In fact, the long term scope of the work done in this project, incorporated with the work done at collaborating universities (Texas A&M and University of Illinois), will culminate into a greenhouse hydroponic system, where the water source is our *scaled* VCC. As shown in Figure 1 below, the vapor compression cycle will feed potable water from the greenhouse air to consumers in a community. From there, the wastewater will be treated and sent back to provide nutrients to a hydroponic greenhouse, which will also provide food for the community. The project goal isn't solely about atmospheric water generation, but a holistic and fully integrated approach to delivering food, water, and energy in an environmentally conscious and clean way.

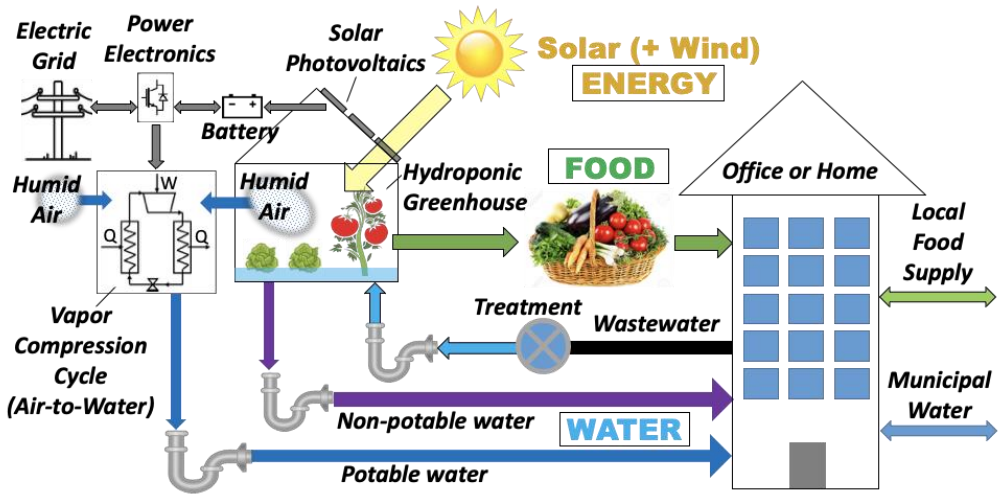

Figure 1: Schematic of holistic project integration and eventual application combining food, energy, and water using the vapor compression cycle.

Available Technology

Dehumidification is the removal of vapor from a gas-vapor mixture, and as it pertains to this project, the separation of water vapor molecules from atmospheric air. There are several methods used for dehumidification that use one of three main technologies: condensing water vapor using cooling surfaces, using sorption materials to absorb/adsorb water vapor (desiccants), and gas separation membranes (Chandler, 2017). The following section reviews various technologies that use a refrigerant in a thermodynamic cycle to cool a surface and condense water vapor in the air. Since this project provides an in-depth, technical understanding of the vapor compression cycle (VCC), the commercial availability of VCC for atmospheric water generation will also be reviewed.

Vapor Compression Cycles (VCC)

The vapor compression cycle is a system containing four major elements, including an evaporator heat exchanger, a compressor, a condenser heat exchanger, and an expansion valve, as shown in Figure 2. These components, in unison, enable the system to condense the medium from vapor form into liquid form through the mechanical work and heat transfer of the aforementioned elements as seen in Figure 3 (Service, 2017). The system interacts, beginning in the evaporator, as such: The temperature inside the evaporator is lower than the ambient temperature surrounding the evaporator, which enables heat transfer from the medium (water, in the scope of the project) to the refrigerant. The now superheated gas refrigerant is compressed in the second stage as a high temperature and high pressure vapor (Welch, 2008). This superheated vapor is then condensed in the third stage, where the high temperature and pressure energy is released to the outside environment. This process is typically catalyzed through the use of a fan, which forces additional airflow over the condenser coils to increase rate of heat transfer from the refrigerant to the ambient air. The condensed vapor is passed through an expansion valve, which reduces the pressure of the refrigerant from condensing pressure to evaporating pressure, thus sub-cooling the liquid (Welch, 2008). The resulting pressure reduction reduces the temperature of the refrigerant in the evaporator allowing the cycle to continue as the low pressure and low temperature refrigerant re-enters the evaporator. Figures 2 and 3below depict the different VCC phases (Cai, Chang, Ding and Zhao, 2013).

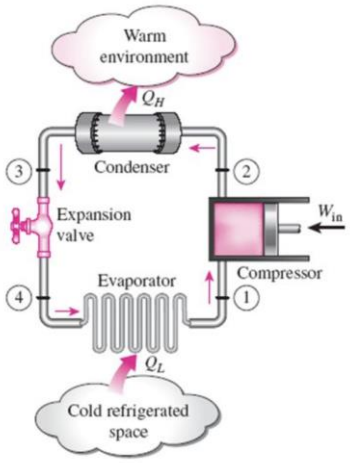

Figure 3: Schematic of an ideal VCC

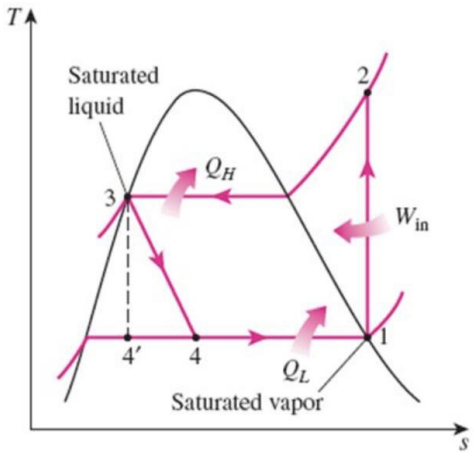

Figure 2: T-s diagram for ideal VCC

Thermal Expansion Valve vs. Capillary Tube

One of the four main components of the system is the device used for refrigerant pressure reduction into a saturated liquid-vapor prior to entry back into the evaporator. There are two widely used technologies, being the thermal expansion valve (TEV), shown in Figure 4 and a capillary tube. The main advantage of a TEV over the capillary tube system is that the TEV is mechanically adaptive to control refrigerant flow to the evaporator based on real time ambient temperature conditions, whereas the capillary tube is a passive method, or preset based on local ambient conditions. The thermal expansion valve works by sensing the temperature of the evaporator using the remote bulb to mechanically open and close the valve, which then dictates how much refrigerant is output to the evaporator. If the evaporator temperatures increases, the pressure on the spring also increases, which will push down on the spring, opening the valve, and allowing more refrigerant to flow to the evaporator for enhanced cooling ("Ideal Vapor Compression," 2018).

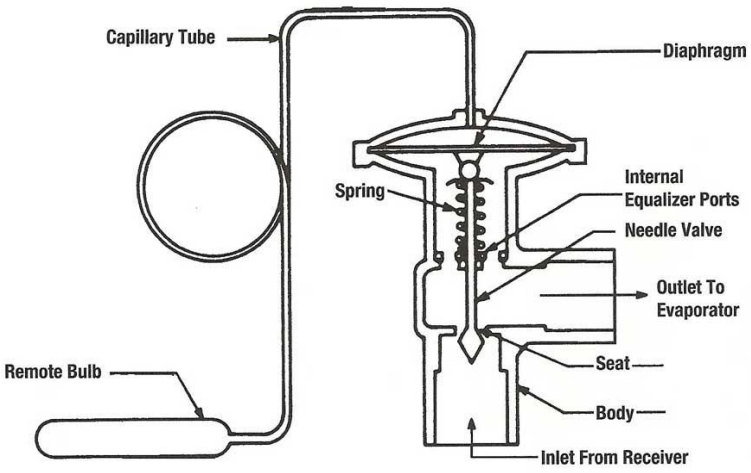

Figure 4: Thermal expansion valve diagram

Competing Technologies

In the following section, competing technologies will be explained and the discussion will include the justification for why the following technologies are not as effective as the VCC for the scope of this project.

Vapor Absorption Cycle (VAC)

Vapor absorption cycles are similar to vapor compression cycles in that they both use an evaporator, condenser, and expansion valve, however the absorption cycle uses thermal energy rather than mechanical energy as the driver. This is done by replacing the compressor with an absorber and generator (shown in Figure 5) which use two working fluids, an absorbent and a refrigerant. The vapor refrigerant exits the evaporator and enters the absorber where it is mixed with a cold absorbent, condensing the refrigerant into a liquid and creating an absorbent-refrigerant solution. A pump then transfers the solution from the low pressure absorber to the high pressure generator. The solution is heated by an external source (solar energy, waste heat, etc.), causing the refrigerant solubility to decrease, driving most of it out of the solution and into the condenser where it completes the cycle through the expansion valve and evaporator, condensing the water vapor from the ambient air. The remaining absorbent is throttled to the evaporator pressure through a second expansion valve and reenters the absorber, completing the cycle (Kirkpatrick, 2017). This cycle works on the basis that "liquid absorbents can attract and retain the vapor phase of a refrigerant at a relatively low temperature, and that vapor solubility in an absorbent solution decreases as the solution temperature is increased", which is why the refrigerant is absorbed at a low pressure and temperature, and released at a high temperature and pressure (Kirkpatrick, 2017). Ammonia-water or lithium-bromide are typical absorbents, both of which cause safety risks, as ammonia is toxic and lithium-bromide is corrosive and creates hydrogen gas when in contact with ferrous materials (Chandler, 2017). The replacement of the compressor with the absorption equipment, and the usage of dangerous absorbents, makes the design of vapor absorption systems much more complex and requires more space and equipment, which is why it is typically used in larger industrial applications. As such, this technology is not as feasible or advantageous as the VCC for a hydroponic operation.

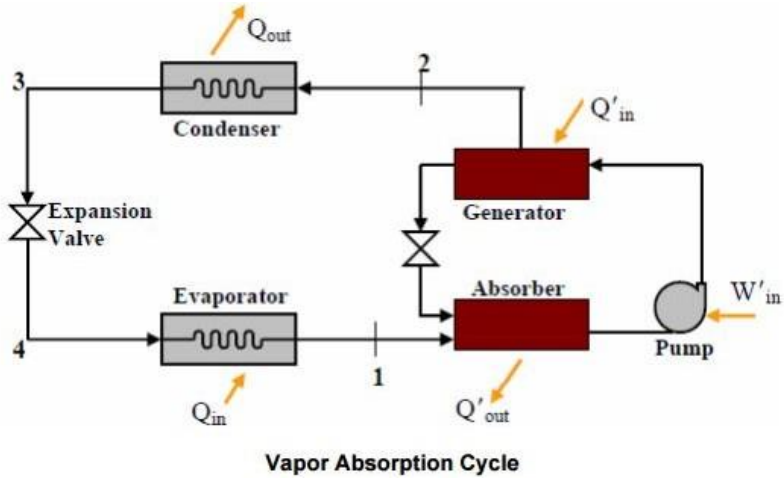

Figure 5: Vapor absorption cycle schematic

Thermoacoustic Cooling (TAC)

Thermoacoustic systems use sound waves and an inert gas as the refrigerant, often helium, to produce cooling on a surface. A loudspeaker resonates the gas, creating oscillations in temperature and pressure. This creates a temperature difference across a porous stack from the constant compression and expansion of the gas from the sound pressure. This process removes heat from the cold side of the unit, and transfers it through the stack, into the hot side ("Thermoacoustic Refrigeration," n.d.). An example TAC system can be seen in Figure 6. An advantage of thermoacoustic refrigeration is that it often uses helium as the acting refrigerant, which is inexpensive, nontoxic, nonflammable, and has no negative environmental effects. Despite this advantage over vapor compression systems, thermoacoustic systems need more design improvements to increase the COP to the level of vapor compression systems ("Thermoacoustic Refrigeration," n.d.).

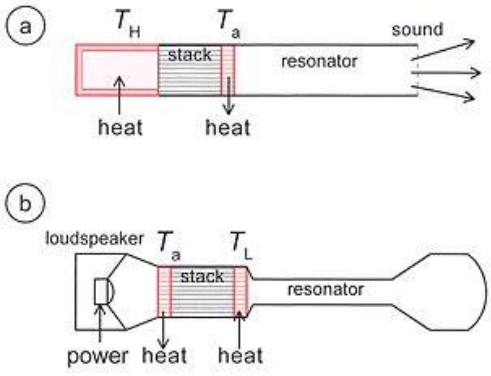

Figure 6: Thermoacoustic cooling schematic

Thermoelectric Cooling (TEC)

Thermoelectric coolers make use of the Peltier Effect to drop the air temperature below dew point and create condensation. The Peltier Effect occurs when a direct current is applied to dissimilar metals and heat is either released or absorbed at the metal junction, depending on the current polarity (Kirkpatrick, 2017). Doped semiconductors are connected electrically in series and thermally in parallel and enclosed by ceramic substrates as seen in Figure 7 (Chandler, 2017). The doping creates either an excess (n-type) or deficiency (p-type) of electrons, where heat absorbed at the cold side and transferred to the hot side of the system is proportional to the current passing through the thermocouples and the number of thermocouples. Heat is absorbed by the electrons at the cold end as they pass from the p-type to the n-type semiconductor. External power to the systems moves the electrons to the hot side, where the heat is expelled to a heat sink at the hot end. The electrons then move from the n-type semiconductor to the lower energy p-type, and the cycle is completed (Atta, 2011). Thermoelectric cooling has many advantages, including no moving parts which require less maintenance, no environmental hazard, and precise temperature control, however they have a lower efficiency than conventional cooling systems and require low heat input, rendering the VCC more attractive for the scope of this project (Chandler, 2017).

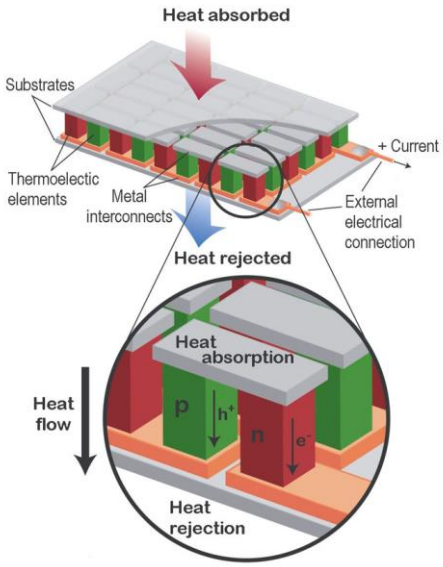

Figure 7: Thermoelectric cooling schematic

Desiccation for Water Generation

Desiccants are sorbents, materials capable of capturing other fluids, which can attract and retain water. Desiccants draw moisture from the surrounding air until an equilibrium is reached, where the air retains a stronger hold on the moisture than the desiccant, or until the desiccant is saturated (Chandler, 2017). Most desiccants use physical adsorption rather than chemical absorption, involving weak van der Waal forces and electrostatic interactions between the air moisture and desiccant surface ("Desiccants: Technical Data," n.d.). Desiccants absorb moisture until saturation or an equilibrium is reached, where they are then heated and a dry air stream is run over them to extract the moisture. The air stream is then run over cooling coils where the water condenses and can be collected. The desiccants then need to be cooled so they can regain their adsorption/absorption capabilities (Chandler, 2017). In liquid desiccant systems, mass transfer between the humid air and the desiccant occurs as a result of the difference in vapor pressure. The equilibrium temperature of the liquid desiccant is determined by the partial pressure of the water vapor in the air (Kirkpatrick, 2017). Similar to a VAC system, the liquid desiccant cycles between an absorber and a generator. The desiccant is sprayed over cooling coils where it absorbs the water vapor and collects in a pool. It is then pumped to the generator and the solution is sprayed over hot coils, separating the water from the solution. This system is generally used in HVAC applications, as a fresh stream of air would then pick up the extracted water and restart the process, where the cool, dry air leaving the absorber would be circulated in the building. Desiccants can also be cycled between VCC system components as seen in Figure 8. For water generation purposes, extra measures need to be taken to ensure that the water separated in the generator can be condensed and used, rather than entering an airstream (Kirkpatrick, 2017). This limitation is incredibly important for water generation and the criticality of the limitation rules this technology out for most effective water generation technique.

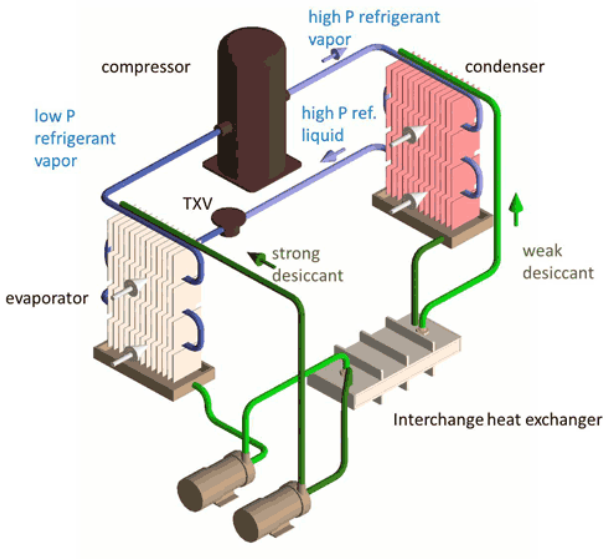

Figure 8: Desiccation system schematic

Gas Separation Membranes

Gas separation membranes are systems that allow certain condensable vapors from a vapor-gas supply to permeate through the membrane. As the vapor-gas supply stream travels through the membrane, only water vapor is allowed to permeate, increasing the water vapor concentration (Chandler, 2017). These systems operate using a constant, positive driving force to maintain supply stream penetration through the membrane. There are multiple methods to do this, the most commercially applicable method being to apply a vacuum to the permeate side as seen in Figure 9 (Kirkpatrick, 2017). This system works by exposing a membrane to a humid air stream that is driven by a vacuum pump which controls the pressure on the permeate side. A heat pump cools the condenser where the water collects into a collection tank. The condenser works as a pressure regulator, as the temperature on the cool surface determines the saturation pressure of the water vapor. A recirculation pump then drives the gas mixture exiting the condenser back through the membrane. Therefore, the driving force of the system is determined by recirculation stream and its water vapor pressure, which is equal to the saturation pressure at the condenser (Muller and Scholz, 2004). Vapor separation membranes can greatly reduce the energy cost of condensing water vapor because only the concentrated water vapor is condensed, rather than the entire air mixture. These systems do have setbacks in atmospheric water generation, because as the ambient air fluctuates in temperature and humidity, membrane surface area must also change to achieve a certain generation rate (Kirkpatrick, 2017). Inflow of non-condensable gases also becomes an issue with large membrane surface areas (Muller and Scholz, 2004). The membrane performance is also hindered as vapor concentrates along the surface of the membrane (Muller and Scholz, 2004).

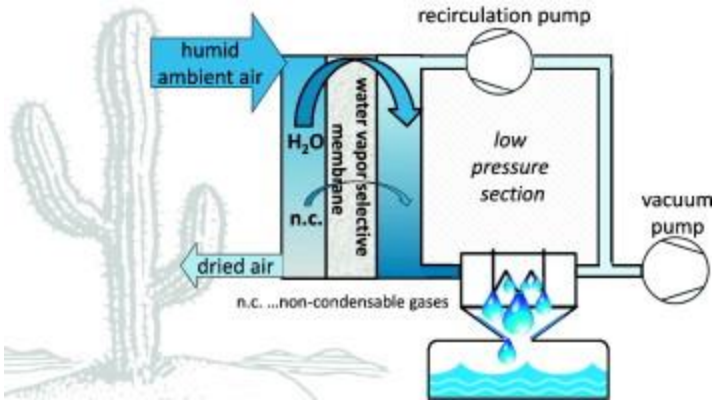

Figure 9: Gas separation system with vacuum as driving force

Table 2 below summarizes the different technologies used for atmospheric water generation and their applications:

Technology	Pros	Cons	Typical COP	Typical Size
VCC	Evaporator temperature easily controlled, efficient, variety of refrigerants can be used	Hazardous refrigerant, must ensure no leaks, wear in the compressor if liquid enters	3-5	Small - Large Domestic - Industrial applications
VAC	Low mechanical work, uses outside heat source, low maintenance	Dangerous refrigerants, large setup, high initial cost	1-2	Large Industrial applications
TAC	Inexpensive & safe refrigerant (helium), no moving parts, close temperature control	Not efficient, can't obtain high Q values	<1	Small Milliwatts - thousands of watts
TEC	No moving parts (less maintenance), no environmental hazards, precise temperature control	Not efficient, can't obtain high Q values	<1	Small Milliwatts - thousands of watts
Desiccation	No refrigerants needed, can be incorporated in VCC and VAC	Water usually carried away in dry air stream, extra measures need to be taken to condense water vapor	Depends on system it is used in	Large Building HVAC systems
Gas Separation	Concentrated water vapor, less energy to condense	Membrane efficiency decreases with larger water vapor volumes, membrane surface area is constant	3-5	Small Magnitude of tens of kilowatts

Table 2: Technology comparison

Emerging Technology

Research teams from the University of California Berkeley and Massachusetts Institute of Technology (MIT) developed a technology to pull water straight from air. Rather than first identifying a societal need, the Berkeley team made huge advances in the chemistry and creation of Metal Organic Frameworks (MOFs) for the sake of advancing science. In the early 2010's the team at Berkeley developed out the technology extensively enough that they recruited the MIT team to attempt to pull water straight from the air.

The MOF technology includes a crystalline structure composed of organic links and inorganic units, being metal ions, to make highly porous structures (continuous 3D networks). Specifically, organic and metal ions are mixed in liquid form, then the liquid is evaporated leaving a powdery substance containing a large and porous framework or crystalline structur, the MOF. The benefit of this structure is that liquid will bind to the framework/interior of the pores. The molecules that bind to the structure will depend on the metal ions that are mixed with the inorganic compounds. In this way, the humidity is not a major contributing factor in absorptivity of the MOF because it is driven largely by electrical charge and attraction. As such, this technology is highly effective even in low humidity environments (<30% humidity) (Cordova, Furukawa, O'Keeffe and Yaghi, 2013).

One of the most critical applications identified for this technology is delivering water to arid regions, in-situ. The proposed solution is a simple one constructed of an adsorption chamber and two heat exchangers as shown in Figure 10.

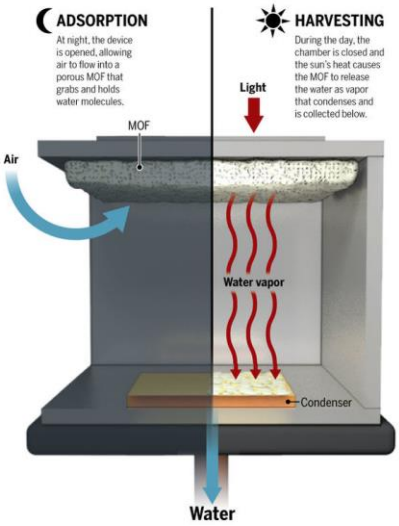

Figure 10: MOF schematic

Here, the MOF material is designed such that it is hydrophilic or water attracting so that during night time, the chamber will remain open and water will absorb into the porous structure from ambient air. During the day time, the chamber will close and the top surface, painted black, will attract sunlight (heat) and allow the water molecules to excite, exiting the MOF as water vapor and moving toward the condenser plate at the bottom of the system. The condenser plate will be exposed, on the bottom side, to ambient outside air and will not have a high thermal conductivity. In this way, water vapor will contact

the condenser plate and begin to condense into liquid water droplets. Finally, the water will flow down through openings in the bottom of the chamber into collection tanks (Chandler, 20).

This technology has significant upsides including that preliminary testing has proven that 1 kilogram of a hydrophilic MOF is able to capture nearly 3 liters of water per day. This is a significant advancement in water collection technology, however, there are downsides. The first being the cost of the MOF, which is roughly $150 per kilogram, not to mention the cost of development and construction of the full system, which has yet to be determined. The second being that this system runs on a very cyclical basis where water is only available after the full day-night process has completed, whereas competing technologies, like a VCC, is able to condense water from air continuously. It is important to note that scientists estimate the atmosphere contains approximately 13 trillion liters of water captured as vapor. This technology paired with other continuous processes could yield incredible results in terms of harnessing and harvesting the potential in the world surrounding us (Service, 2017).

Summary of VCC Governing Equations

In order to better understand the VCC, it was important to gather the key equations that explain the thermodynamic principles occurring at each phase.

Compressor: Stage 1 → 2

The compressor can be sized by determining the amount of work needed to raise the enthalpy of a certain amount of refrigerant.

Equation 1: $W_c = \dot{m}(h_2 - h_1)/\eta$

Where W_c is compressor work, $\dot{m}$ is the mass flow rate of the refrigerant, and h_2 and h_1 is the refrigerant enthalpy exiting and entering the compressor respectively. This yields a kW rating for the compressor. Ideally, the enthalpy entering the compressor would equal the enthalpy at the saturation pressure so that the refrigerant enters as a saturated vapor. This ensures that no liquid forms in the compressor, which would cause wear. A suction line accumulator is commonly used to achieve this, as explained later in this section. The work of the compressor can also be related to the inlet and outlet pressure difference using its isentropic efficiency.

Equation 2: $W_c = \dot{m}RT_1(k/k-1)[(P_1/P_2)^{k-1/k}-1]/\eta$

Where R is the universal gas constant, T_1 is the inlet temperature, k is a constant (1.4) for isentropic conditions, P_1 and P_2 are the inlet and outlet pressures respectively, and η is the isentropic efficiency, which compares the actual compressor work to the compressor work if there was no change in entropy.

Condenser: Stage 2 → 3 and Evaporator: Stage 4 → 1

The condenser and evaporator heat exchangers manipulate pipe diameter and length to accept or reject heat to the ambient air. This relationship is shown in the equations below.

Equation 3: $Q = UA(\Delta T)$

Equation 4: $Q = \dot{m}h_{fg}$

Where Q is the total heat lost/gained, U is the conductance, A is the surface area, and ΔT is the difference in temperature between the flowing refrigerant and ambient air. The second Q equation describes a phase change of the refrigerant in the evaporator and condenser, where the heat lost/gained equates to product of the mass flow rate and latent heat value (h_{fg}). Overall conductance is defined as the heat exchangers UA value, which identifies the overall resistance to heat transfer. This includes the convective resistance of the refrigerant, the conductive resistance of the heat exchanger pipe, and the convective resistance of the outside air, shown in that respective order in the equation below.

Equation 5: $1/UA = 1/h_i \pi D_i L + ln(D_o/D_i)/2\pi kL + 1/h_o \pi D_o L$

For the evaporator, the final term Equation 5 can be ignored since the evaporator surface temperature is known. The internal convection for a vertical evaporator is found using the Coulson McNelley correlation and relating it to the Nusselt number:

Equation 6: $Nu = (1.3+39D_i)[Pr_l^{0.9} Re_l^{0.23} Re_v^{0.34} (\rho_l/\rho_v)^{0.25} (\mu_v/\mu_l)]$

Equation 7: $Nu = hD_i/K$

The Cavallini Zecchin correlation is used for the condenser, which determines the internal convection coefficient for condensation as:

Equation 8: $h = (K/D_i)0.05Re^{0.8}Pr^{0.33}$

Where Re is the two phase Reynolds Number, which is solved for by determining the vapor and liquid phase Reynolds Numbers as follows:

Equation 9: $Re = Re_v (\rho_l/\rho_v)^{0.5} (\mu_v/\mu_l) + Re_l$

Where Re_v and Re_l are the vapor and liquid Reynolds Numbers, respectively, calculated by:

Equation 10: $Re_{v/l} = 4\dot{m}/\pi D_i \mu_{v/l}$

By combining the last two equations, one can make a conclusion on the different ways to increase the rate of heat transfer:

- Increase the convection coefficient of air (h_o) by using forced convection from a fan
- Increase the surface area of the pipe by increasing length, outer diameter, or adding fins. The pressure drop across the condenser and evaporator will constrain these values.
- Increase the pipe conductivity (k) by changing the pipe material and thickness.

Expansion Valve: Stage 3 → 4

Refrigerant expansion is an adiabatic process, meaning Δh = 0. As previously stated, the expansion valve serves to drastically reduce the refrigerant pressure, and therefore the refrigerant temperature, so that a cold liquid enters the evaporator for optimal heat extraction from the ambient air and cooling of the evaporator surface.

Refrigerant Selection & Justification

A typical refrigerant used in common refrigeration cycles is R-134a, which is a hydrofluorocarbon (HFC). HFC's generally have high global warming and ozone depletion potential, which is not ideal or in keeping with the purpose of delivering clean water in a sustainable way. As a result our team researched a more sustainable and less harmful refrigerant alternative with similar thermodynamic properties as R-134a. We discovered a new generation of refrigerants known as hydrofluoroolefin (HFO) refrigerants that exhibit much lower global warming and ozone depletion potential as compared with their HFC counterparts. Accordingly, we discovered HFO-R1234ze, which is produced by Honeywell, as a drop in replacement for R-134a with the traditional enhanced sustainability qualities of an HFO. For example, HFO-1234ze has a low boiling point, low operating pressure, and low GWP ("Refrigerant HFO-1234yf," 2018). The sustainability enhancements and similarities are displayed in Table 3 below.

Refrigerant	Boiling Point (°F/°C) at 1 atm.	Liquid Pressure at 0°C (kPa/atm)	Global Warming Potential (CO_2=1)
R-134a	*-14.9/-26*	*191.7/1.89*	*1430*
R-1234ze	*-2.2/-19*	*115.2/1.14*	*6*

Table 3: Sustainability and thermodynamic properties of refrigerant options

These two refrigerants operate similarly in refrigeration systems, however, will require slight modification in the design cycle of the VCC. That being said, the tradeoff is worth the vast difference in global warming potential to create a sustainable system with the lowest carbon footprint at similar price points of the refrigerant. Additionally, most of the equipment used in R-134a systems can be retrofitted for use with R-1234ze, so there is no additional costs associated with hardware selection.

Assumptions and Parameters Assumed

Thermodynamic States and Operating Pressures:

For calculation purposes, it was assumed that the refrigerant would fully evaporate in the evaporator and enter the compressor as a vapor. It is imperative that only vapor enters the compressor, as liquid droplets can cause compressor wear and damage. To ensure this, the actual evaporator length was tripled from the calculated value, as seen in the *Design* section. For the internal convection coefficient in the evaporator, it was assumed that a liquid-vapor mixture entered the system for use in the two-phase evaporation correlation. The vapor quality was estimated using the R-1234ze pressure-enthalpy graph at the operating pressures. It was also assumed that there would be no pressure drops across the heat exchangers for ease of simulation.

The low and high operating pressures were also assumed. Ideally, the VCC governing equations would be compiled with "n" equations and "n" unknowns to solve for variables such as low and high pressure, heat exchanger lengths, and compressor work, using a non-linear equation solver such as the "fsolve" function in Matlab. Non-linear equation solvers take user-input initial guesses for unknown variables and iterate

until the values converge. This is the ideal process for system simulation because it minimizes the amount of assumptions that need to be made. Unfortunately, given the project time constraint due to the large amount of time needed for purchasing parts, building the system, and data collection and validation, our group was unable to simulate the system using a non-linear solver. Instead, low and high pressures were chosen based on suggested evaporating and condensing temperatures from the Performance Data Sheet for the compressor to be used in our system, as seen in Figure 11 below.

Tecumseh

Performance Data Sheet

AEA3414YXA

General Information

Model	AEA3414YXA	**Refrigerant**	R-134a
Test Condition	ARI	**Performance Test Voltage**	115V ~ 60HZ
Return Gas	18.3°C (65°F) RETURN GAS	**Motor Type**	RSIR

Performance Information

Evap Temp (°F)		Condensing Temperature (°F)				
		100	110	120	130	140
20	Btu/h	959	857	770	686	592
	Watts	179	183	184	184	184
	Amps	2.50	2.50	2.51	2.51	2.50
	Lb/h	13.3	12.4	11.7	11.0	10.0
25	Btu/h	1080	969	870	774	669
	Watts	189	193	196	197	198
	Amps	2.48	2.50	2.52	2.54	2.55
	Lb/h	15.1	14.1	13.3	12.5	11.5
30	Btu/h	1230	1100	994	887	771
	Watts	199	204	208	210	213
	Amps	2.52	2.55	2.58	2.61	2.64
	Lb/h	17.2	16.2	15.3	14.5	13.4

Figure 11: Performance data sheet

The low pressure side of the compressor was calculated to be 179.4kPa based on the evaporator surface temperature being set to 5°C (~20°F) to enhance the evaporator's ability to condense liquid water on the surface without dropping below freezing where frost would form. The high pressure side of the compressor was assumed to be 780kPa based on R134a high temperature compressors, which are highly suitable for our R1234ze refrigerant based on the Performance Data Sheet. The corresponding condenser temperature is 41°C (~110F), which is about 20°C above the outside air temperature, where the heat will be expelled.

Heat Exchanger Material Selection:

It was decided to use copper tubing due to its reasonable pricing as well as its ability to withstand the operating pressures. A summary of the heat exchange (per hour) and tube size is tabulated in Table 4 below. Given estimates that operation is between 10K-20K Btu/H a ¼' in. diameter copper tube can be used, however ⅜" tubing was chosen to increase the factor of safety in the event that unintended high pressures occur in the system. Table 5 below also shows the internal pressure limits (psi) for copper tubing, further verifying that the ⅜" in. tubing will not fail at the operating pressures.

Tubing	BTU/H	GPM	Pipe Size (In.)
Copper	10K - 20K	2 - 4	1/4”
	20K - 45K	4 - 9	1”
	30K - 80K	6 - 16	1 1/4”
	50K - 105K	10 - 21	1 1/2”
	100K - 225K	20 - 45	2”
Multi-Layer Composite (MLC)	10K - 20K	2 - 4	3/4”
	20K - 45K	4 - 8	1”
PEX (Wirsbo he,PEX™ & Uponor)	2.5K - 10K	0.5 - 2	1/2”
	5K - 15K	1 - 3	3/4”
	15K - 25K	3 - 5	1”
	20K - 45K	4 - 9	1 1/4”
	30K - 70K	6 - 14	1 1/2”
High Density Polyethylene (HDPE)	75K - 205 K	15 - 41	2”
	150K - 575K	30 - 115	3”
	250K - 1,125K	50 - 225	4”

Table 4: Copper tubing size guide (www.supplyhouse.com)

Rated Internal Working Pressures for Copper Tube Types K, L & M

Size	TYPE K		TYPE L		TYPE M	
Inches	Annealed	Drawn	Annealed	Drawn	Annealed	Drawn
Service Temperature up tp 150° F (5,100 psi, annealed; 9,000 psi drawn)						
1/4	900	1595	810	1350	-	-
3/8	990	1745	675	1195	475	840
1/2	780	1375	625	1105	430	760

Table 5: Copper tubing working pressures

Ambient Assumptions:

The VCC is to be run in an indoor lab. Therefore, it is assumed that the evaporator and condenser will be accepting/rejecting heat to the indoor lab air. Using ASHRAE indoor air quality standards 55-2013 and 62.1-2016, it was assumed that the ambient air is 70°F and 50% relative humidity. Indoor air is typically much drier than outside air, so using these values will ensure that the device will successfully operate if placed outside at similar temperatures.

Nominal Assumptions & State Points

Property	**Value**	**Comments**
Pressure 1	179.4 kPa	Pressure at -5°C
Temperature 1	-5°C	Refrigerant Temp. through evap.
Enthalpy 4	193.42 kJ/kg	Assuming saturated liquid
Enthalpy 1	380.73 kJ/kg	At P1,T1
Enthalpy hfg	195.810 kJ/kg	State point 1
Density of liquid R1234ze	1254.56 kg/m^3	State point 1
Density of vapor R1234ze	9.70 kg/m^3	State point 1
Viscosity of liquid R1234ze	286.19 * 10^{-6} Pa*s	State point 1
Prandtl Number	4.4	State point 1
Liquid Thermal Conductivity of R1234ze	84.902*10^{-3} W/m*K	State point 1
Internal Diameter of Copper Pipe	.0104 meters	
External Diameter	.0127 meters	
Pressure 2	780 kPa	Pressure at 41.49°C (Reasonable condensing temperature)
Enthalpy of Vapor R1234ze	410 kJ/kg	State point 2
Specific Heat of R1234ze	1.0545 $kg*m^2/K*s^2$	State point 2
Thermal Conductivity of R1234ze	.0689 W/m*K	State point 2
Density of liquid R1234ze	1110 kg/m^3	State point 2
Density of vapor R1234ze	41.38 kg/m^3	State Point 2
Viscosity of liquid R1234ze	145.97 *10^{-6} Pa*s	State Point 2
Viscosity of vapor R1234ze	12.96*10^{-6} Pa*s	State Point 2
Prandtl Number	3.47	State Point 2
Compressor Efficiency	80%	

Table 6: Nominal assumptions and state points

Design

The VCC governing equations, refrigerant properties, and assumed parameters supplied adequate information to design the VCC system using the Matlab equation solving software. The first design step was determining the necessary evaporator length using ⅜" copper tubing. Using the amount of water to be condensed (500cc/hour) and the saturation temperature of the ambient air was the starting point in the evaporator design. The total heat into the evaporator was determined by applying Equation 4 to the amount of water being condensed, and using the R-1234ze latent heat property, the refrigerant mass flow rate could be determined by equating the two.

With the refrigerant mass flow rate solved for, the evaporator length could be found by using Equations 3 and 5. Equations 6 and 7 were used to model the internal convection coefficient used in Equation 5.

Knowing the refrigerant thermal conductivity at the assumed pressure and the pipe internal diameter, the internal convection could be solved for and the evaporator length can be determined using Equation 4. The calculated length was 0.32 meters. As stated in the *Assumptions and Parameters Assumed* section, the actual evaporator length was tripled to ensure adequate length for water condensation and refrigerant phase change, resulting in an actual length of 0.96 meters. A vertical configuration was chosen for the evaporator to assist with the collection of condensed water on the surface. Water on the surface will fall and accumulate on the bottom of the tubing, making it easier to drip off and collect. In a horizontal configuration, an equally distributed, thin film of water would collect along the tube surface, making it harder to collect. The use of gravity to force water off the tube would not be possible and an external piece of equipment, such as a fan or vibration device, would be needed for water collection. 0.32 meters is a satisfactory length, given the relatively small amount of heat input of 0.3457 kW into the evaporator, as detailed in the *Design* section. Furthermore, the tripled length of 0.96 meters will fulfill the geometric constraints of having to fit into a tabletop device, given the vertical configuration.

The same procedure was used in solving for the condenser length. Equation 8 was used to solve for the internal convection coefficient, where Equations 9 and 10 were used to solve for the two phase Reynolds Number in Equation 8.

The resulting condenser length was 0.67 meters. The actual condenser length was also tripled to ensure full phase change from vapor to liquid and to account for sensible heat loss from the superheated state of the vapor exiting the compressor, resulting in an actual condenser length of 2.01 meters. With the added work from the compressor, it is expected to have a higher condenser length when compared to evaporator length. The vapor exiting the compressor will also be in a superheated state, so the tripling of the calculated length will account for the sensible heat loss from the superheated to the saturated state before phase change can occur. Since the condenser is significantly longer than the evaporator, a vertical orientation is suggested to fit the geometric constraints. A vertical orientation is also desirable for the use of ice water in aiding the refrigerant phase change, as outlined later in the *Experimental Setup* section.

The next design step was sizing and sourcing a compressor. Using Equation 2, the resulting compressor work was about 115 watts to raise the pressure from 180kPa to 780kPa. As previously shown on the Performance Data Sheet in Figure 11, an R-134a Tecumseh compressor was chosen, with a maximum

power output of 550 watts, which is well above the required power. Since R-1234ze is a new refrigerant, there aren't any easily accessible compressors made specifically for R-1234ze. Since "R-1234ze(E) will show operating conditions and applied costs much more in line with R-134a according to system and compressor sizes", it was decided to use an R-134a compatible compressor ("Solstice® ze Refrigerant", 2017).

The equations used in the design process are outlined in Table 7 below.

Results

Equation	Calculation	Comments
$P_{vap} = \phi P_{sat}$	$P_{sat}@T_{sat} = 20°C = 2.339\ kPa$ $P_{vap} = \phi P_{sat} = .67(2.339)$ $\mathbf{P_{vap} = 1.567\ kPa}$	
$T_{sat}@P_{vap}$ = Evaporator Surface Temperature	$T_{sat}@P_{vap} = 13.7°C$ $\mathbf{T_{surface} = 5°C}$	$T_{surface}$ is set lower in order to enhance water generation on evaporator surface
$Q_{in} = \dot{m}_{water}\Delta h$	$\dot{m}_{water} = (500cc/hr)(1hr/3600s)(1kg/1000cc)$ $\dot{m}_{water} = .000139\ kg/s$ $\Delta h = h_{fg}@T_{sat} = 5°C = 2489.1\ kJ/kg$ $Q_{in} = \dot{m}_{water}\Delta h$ $Q_{in} = (.000139kg/s)(2489.1\ kJ/kg)$ $\mathbf{Q_{in} = 0.3457\ kW}$	
$\dot{m}_{refrigerant} = Q_{in} / h_{fg}$	$\dot{m}_{refrigerant} = 0.3457kW / 195.81\ kJ/kg$ $\mathbf{\dot{m}_{refrigerant} = .001765\ kg/s}$	
$1/UA_e = 1/(h_{ie} * \pi * D_i * L) + (\ln(D_o/D_i)/(2 * \pi * k * L)$	$\mathbf{UA_e = 34.57\ W/m^2K}$ $\mathbf{L_e = 0.323\ m}$	See Appendix 1 for formulation and derivation of equations
$h = (K/D_i)0.05Re^{0.8}Pr^{0.33}$	$\mathbf{h_{ic} = 3118.3\ kJ/kg}$	
Solutions for h_2, T_2, UA_c, & L_c from Matlab script	$\mathbf{h_2 = 421.4\ kJ/kg}$ $\mathbf{T_2 = 41.5°C}$ $\mathbf{UA_c = 21.43\ W/m^2K}$ $\mathbf{L_c = 0.67\ m}$	See Appendix 2 for formulation and derivation of equations
$Q_{out} = UA_c \Delta T$	$Q_{out} = (21.43\ W/m^2K)(21.5K)$ $\mathbf{Q_{out} = 0.4607\ kW}$	
$W_c = Q_{out} - Q_{in}$	$W_c = 0.4607kW - 0.3457kW$	

	W_c = 0.115 kW	
COP = Q_{in} / W_c	COP = 0.3457 kW / 0.115 kW **COP = 3.01**	

Table 7: Results for Governing Equations

Design Results Discussion

Several parameter assumptions had to be made during the design of the heat exchangers. Ideally, the high and low side pressures would not be assumed but instead solved using a non-linear equation solver, such as the "fsolve command" in Matlab. The resulting refrigerant properties, such as density, viscosity, Prandtl number, and thermal conductivity would need to be curve fit in terms of the operating pressures. This was attempted during the design phase of the project, however a solution that converged to realistic values was not reached. In order to stay on track with the project timeline, the operating pressures were then assumed using the Tecumseh Performance Data Sheet, as outlined in the *Assumptions and Parameters Assumed* section. Convergence using a non-linear equation solver would eliminate the need to make any assumptions and would yield ideal optimized results to maximize system performance. However, since convergence was not reached, tripling the heat exchanger lengths given reasonable parameter assumptions will ensure that there is adequate length for full refrigerant phase change.

The low side pressure determined an evaporator internal temperature of -5°C (21°F). Although this value is somewhat arbitrary in the scope of this project, it falls within freezing temperature and saturation temperature, so it will prove to be effective in condensing water vapor. This value served as the basis for our calculations for determining the heat entering the system from the ambient air. The high pressure side of the system was assumed to be 780kPa based on the Performance Data Sheet results for R-134a high temperature compressors. The corresponding condenser temperature is 41°C (~110F), which is about 21°C above the ambient air temperature where the heat will be expelled. Accordingly, this is an appropriate assumption given the system will be built such that a variable throttle valve will be used on the high pressure side paired with a barometer to set the operating pressure to the desired 780kPa.

The only concern from the results is the low *UA* value for the condenser. Since the heat rejected at the condenser side is the sum of the heat into the evaporator and the compressor work, it is expected that the condenser *UA* value be higher than that of the evaporator. One explanation for this low value is the superheated vapor temperature exiting the compressor, which then drops about 10°C before phase change occurred, at a temperature 21°C above ambient. Since $Q = UA\Delta T$ and the temperature difference between refrigerant and ambient conditions was much greater on the condenser side, the smaller *UA* value can be accounted for in the calculations.

Ethical Considerations

A vital aspect of a successful engineering system design is following and utilizing the ethical guidelines set forth by pertinent professional institutions. The first fundamental canon of engineering set by the National Society of Professional Engineers is to "Hold paramount the safety, health, and welfare of the

public" ("NSPE Code of Ethics", 2018). This is of paramount importance for this system given the high operating pressures, flammable refrigerant, and future applications in hydroponic systems.

The American Society of Heating, Refrigerating, and Air-Conditioning Engineers, Inc. (ASHRAE) develops standards of ethics and utilization specific to refrigeration applications. Specifically, this section will outline the guidelines defined in ASHRAE 15 - An American National Standard Safety Code for Mechanical Refrigeration. Section 9 of ASHRAE 15 - *System Design Pressure* immediately influenced design requirements for this project, inherently driving purchasing decisions throughout the design phase. The following standards will be referenced throughout the report to fully understand the purpose of those design cycle decisions ("ASHRAE 15", 1994):

9.2.1 "Design pressures shall not be less than pressure arising under maximum operating, standby, or shipping conditions. When selecting the design pressure, allowance shall be provided for setting pressure-limiting devices and pressure-relief devices to avoid nuisance shutdowns and loss of refrigerant."

9.2.1.1 "The design pressure selected shall exceed maximum pressures attained under any anticipated normal operating conditions, including conditions created by expected fouling of heat exchange surfaces."

9.4.1 "Refrigerating systems shall be protected by a pressure-relief device or other approved means to safely relieve pressure due to fire or other abnormal conditions."

9.5.1 "Pressure-relief valves shall start to function at a pressure not to exceed the design pressure of the parts of the system protected."

9.8 "When equipped with a stop valve in the discharge connection, every positive displacement compressor shall be equipped with a pressure-relief device of adequate size and pressure setting, as specified by the compressor manufacturer, to prevent rupture of the compressor or to prevent the pressure from increasing to more than 10% above the maximum allowable working pressure of any other component located in the discharge line between the compressor and the stop valve."

9.9.1 "Pressure-limiting devices shall be provided on all systems operating above atmospheric pressure…"

9.13.2 "Joints on refrigeration-containing copper tube that are made by the addition of filler metal shall be brazed."

Instrumentation & Assembly

In order to verify that the actual system is performing to the calculated standards, temperature, pressure, and mass flow rate readings must be taken. This is done using thermocouples, pressure transmitters, and a flow meter. The piping and instrumentation diagram (P&ID) can be seen in Figure 12 below, which outlines all the necessary equipment for experimental setup.

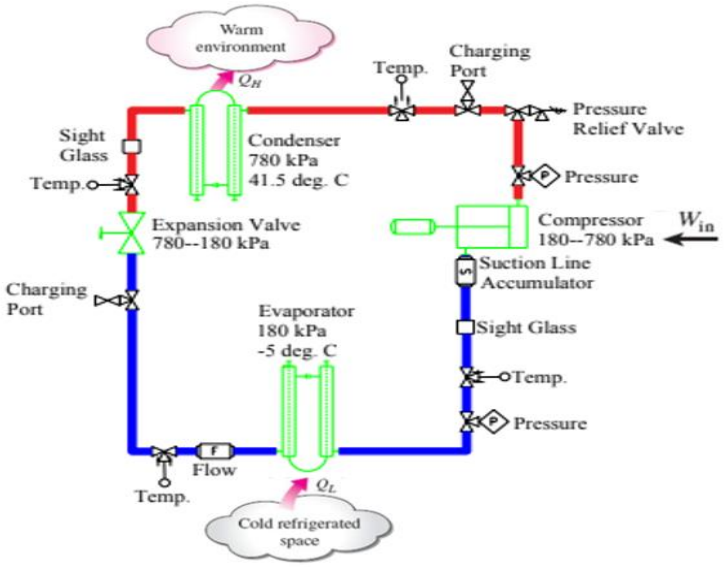

Figure 12: P&ID of experimental VCC

Every piece of equipment, with exception to the inline flowmeter and sight glasses, is connected to the system via a copper tee that is brazed to the copper tubing. Absolute pressure is measured at the inlet and outlet of the compressor to ensure the correct pressure fluctuation on the low and high side of the system. Temperature is read at the inlet of both heat exchangers, the compressor inlet, and the expansion valve outlet. Knowing the high and low pressures, the temperature readings will indicate the phase of the refrigerant at the specific stages in the VCC. Similarly, sight glasses at the entrance of the compressor and exit of the condenser will allow for verification that the refrigerant undergoes a full phase change in both heat exchangers, as the refrigerant should exit the evaporator as a vapor and exit the condenser as a liquid. Two binary valves, labeled as “charge” in the P&ID, are used to charge and discharge the refrigerant from the system, and are also used for system leak testing and vacuuming. A pressure relief valve is also used on the high pressure side of the system as an emergency safety device in the incident that the pressure is raised too high and could damage the equipment. This will allow the pressurized vapor to exit the system, thus relieving some of the pressure. Finally, a suction line accumulator is used right before the compressor inlet. The function of the accumulator is to collect any liquid refrigerant before it enters the compressor so the compressor does not become damaged. Once the liquid is captured, it is vaporized and then cycled back into the system.

All of the equipment requires an adapter at the copper tee. The copper tees are unthreaded, therefore an adapter must be brazed to the tee to allow for a male (MNPT) or female (FNPT) connector, depending on the equipment that is used. This is done by brazing a short piece of copper tubing to the tee, where the adapter can then be inserted and brazed to the system.

Heat Exchanger Fabrication

In order to save table space, it was decided to orient both heat exchangers in the vertical direction. Using the lengths from the *Design* section as a guideline, the evaporator and condenser were cut from a ten foot stock of copper tubing. The actual cut length was slightly greater than the calculated length to leave extra

room on either side of the condenser and evaporator to account for any slight measurement errors. Next, the tubes had to be bent into the desired shape using a hand-held tube bender shown in Figure 13 below.

Figure 13: Tube bending device

Tubing was inserted through the black slot shown in the figure and bent using the apparatus at the end of the black handle section. The final configurations for the evaporator and condenser are shown in Figures 14 and 15.

Figure 14: Evaporator tubing

Figure 15: Condenser tubing

Brazing

Brazing is performed by melting a brazing alloy between two pieces, which then cools and solidifies to form the connection. First, the surfaces that are in contact are sanded so that paste flux can be applied and

stick to the surfaces as shown in Figures 16 and 17. The paste removes the last layer of oxidized metal when melted to form a stronger brazed joint.

Figure 16: Paste flux application

Figure 17: Tubing with paste flux

Once paste flux is applied to both surfaces, the pieces are connected and heated using a blow torch. The brazing alloy can now melt and solidify around the connection. This process is depicted in Figures 18 and 19.

Figure 18: Brazing application

Figure 19: Brazing application cont.

Brazing is the most cost effective way to add adapters and connections into the system, as there is no need to purchase extra fittings for threaded connections. Threaded adapters are brazed to the ends of all the tees to account for the various instruments depicted in the P&ID. Shown below is the evaporator section, ready for leak testing with all the instruments installed. The flow meter and thermocouple to the right of the evaporator in Figure 20 correspond to the icons to the left on the P&ID. Similarly, the pressure transmitter, thermocouple, and sight glass to the left of the evaporator in the figure correspond to the icons to the right on the P&ID.

Figure 20: Evaporator with instruments added

The same configuration is shown for the condenser in Figure 21 below. The instruments at the entrance of the condenser are shown on the right in the figure and those at the exit are shown to the left in Figure 21.

Figure 21: Condenser with instruments added

Once the heat exchangers were fully fabricated with the instruments, the expansion valve section of the system was added, shown in Figure 22 below. The entire loop before it was brazed to the compressor is shown in Figure 23.

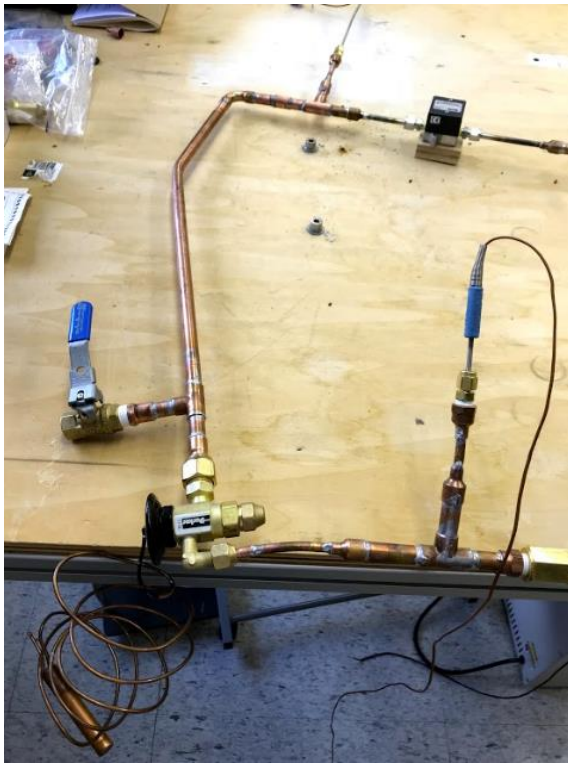

Figure 22: Expansion valve

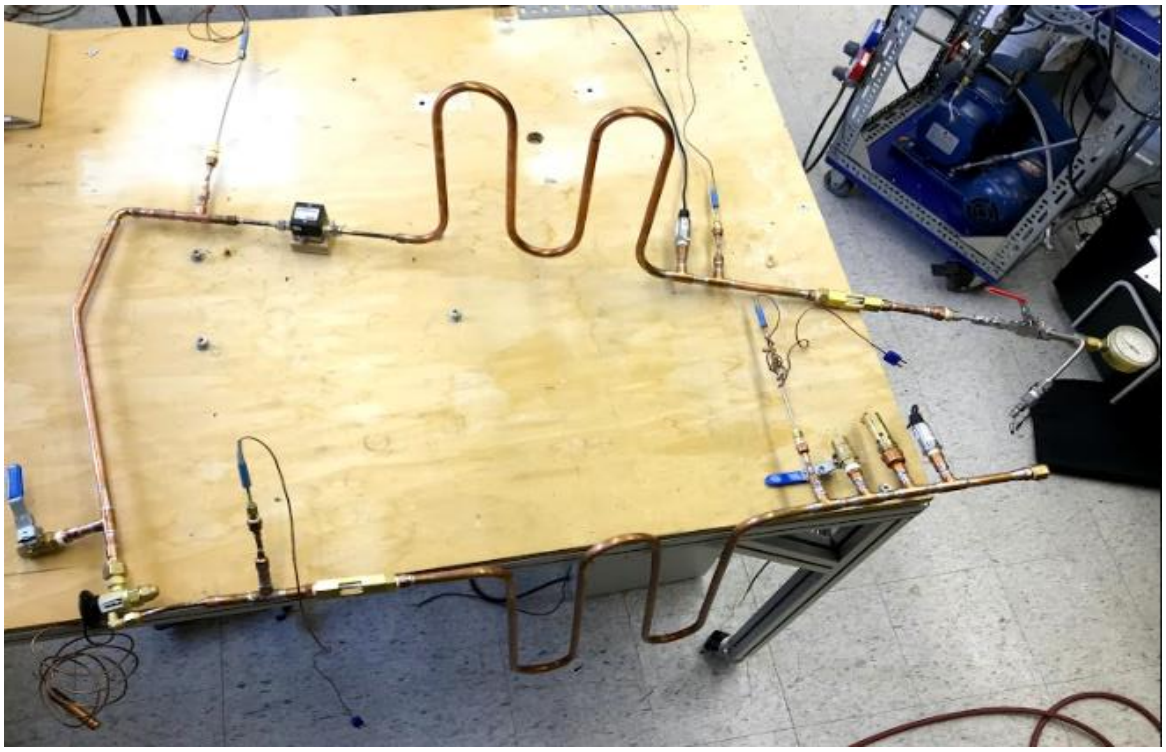

Figure 23: Full system assembly (without compressor)

Leak Testing

As mentioned in the previous section, each part of the system must be leak tested before it is fully integrated. This ensures that no refrigerant in vapor form will escape during operation. Leak testing involves filling a section with compressed air and capping the other end to trap the air, as seen in Figures 24 and 25 below.

Figure 24: Leak testing

Figure 25: Leak testing cont.

Once the section is filled, soapy water is sprayed at each brazed and threaded connection to check for a leak. If a leak is present, bubbles will form where the water was sprayed and the pressure will drop over time. If a leak occurs, the threaded connection must be tightened or additional brazing alloy must be added to fix the leak. The evaporator and condenser sections were capped and tested separately. Since the

condenser will be operating at 7.8 bar, leak testing was performed slightly above this pressure, at about 8.5 bar, to make sure the equipment would hold up during operation. During this process, the pressure relief valve was also tested to make sure it was operating properly. The relief valve was preset to 8.5 bar, so when that pressure is reached, a seat at the base of the valve is opened, allowing vapor to escape. Once the expansion valve section was added, the entire system was leak tested again. Insulation was then added to prevent any heat loss between the heat exchangers, as shown in Figure 26 below.

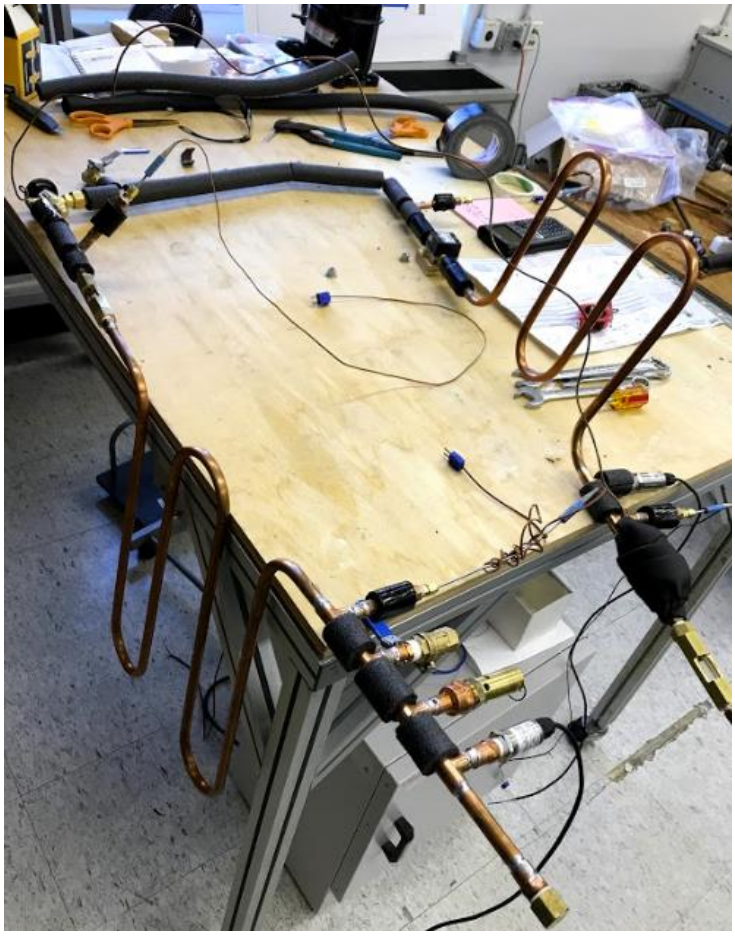

Figure 26: System loop with insulation

Compressor Wiring

The final step in the system assembly was powering the compressor. Since the Tecumseh compressor is resistance start, induction run (RSID), there is no need for an external start or run capacitor. A capacitor is used to alter the current received by the motor, where it would be increased to start the motor due to the high starting torque requirements, and then lowered once the motor moved to a steady-state running phase. RSID motors don't require capacitors, so wiring is relatively simple. Figure 27 below shows a wiring diagram for an RSID motor.

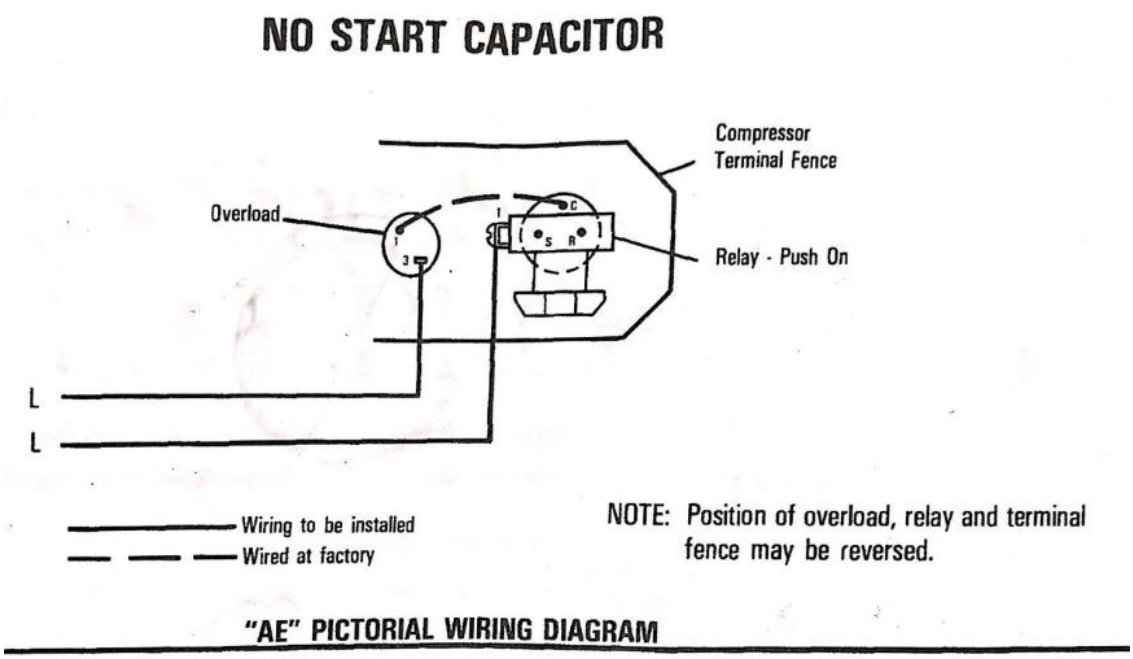

Figure 27: RSID wiring diagram

As shown in the figure, line power is applied to run winding and overload capacitor, and the system is grounded on the compressor. The actual system wiring is shown in Figure 28 below

.

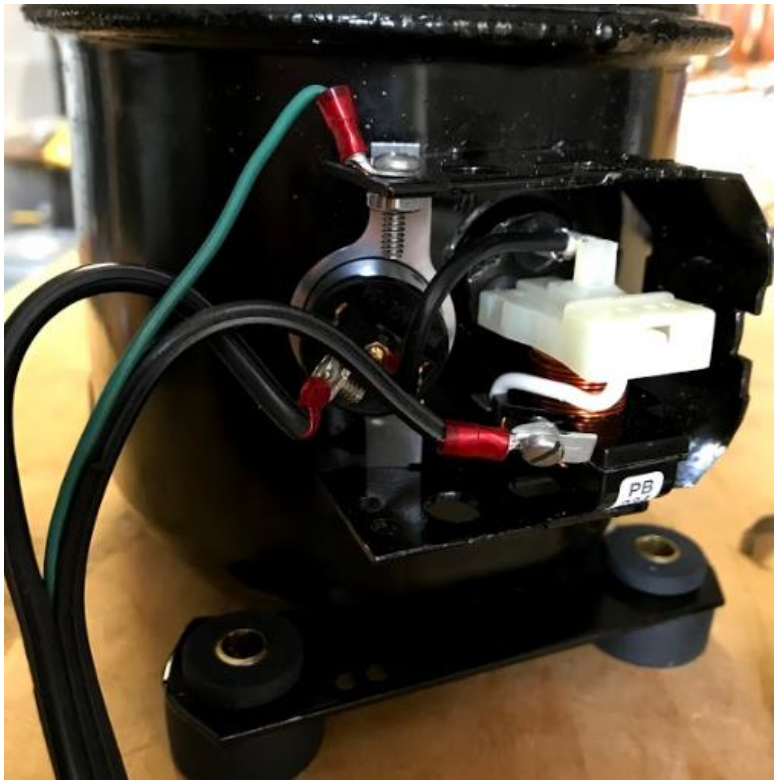

Figure 28: Wired compressor

The two black wires in Figure 28 are line power with the green as ground. These wires lead to a three prong outlet plug-in so the compressor can be run from almost any location.

Experimental Setup

After the final leak test was performed, the exit of the evaporator and entrance to the condenser was brazed to the compressor, along with the suction line accumulator, as seen in Figure 29 below.

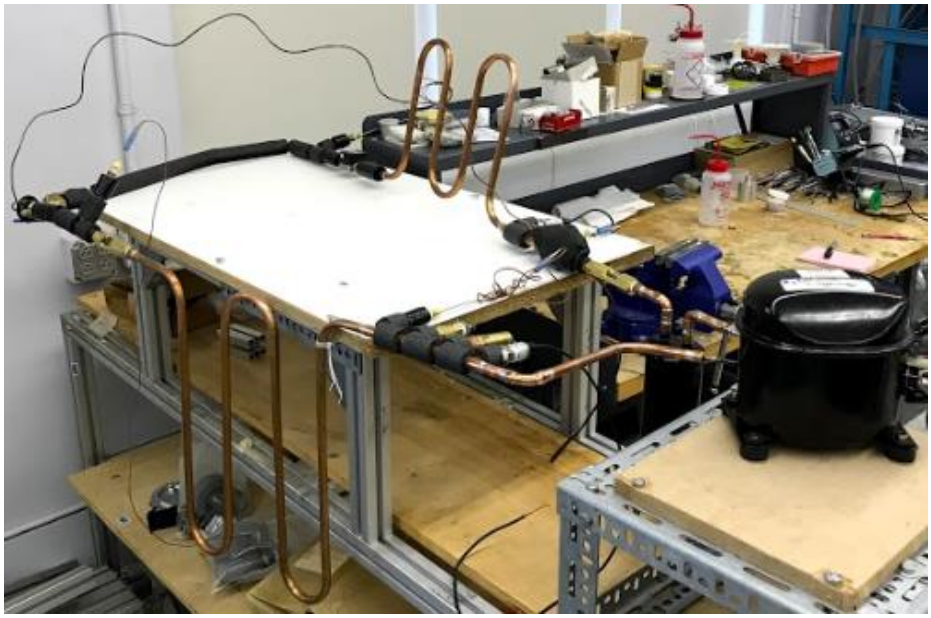

Figure 29: Fully assembled VCC

The final step before fully running the system was to clean the inside of the tubing of any debris and dirt so that it would not affect the system performance and damage the equipment. To do this, the system was first vacuumed to about 150 microns to remove all the air so that it does not mix with the refrigerant. The refrigerant canister was then connected to a manifold that leads to one of the binary valves in the system and a refrigerant recovery unit. The manifold controls whether refrigerant flows from the canister to the system or from the system to the recovery unit. Once loaded with refrigerant, the equipment was rotated and moved around so that refrigerant flowed through every part of the system. It was then flushed out through the recovery unit and the system was ready for testing. The cleaning setup can be seen in Figure 30 below.

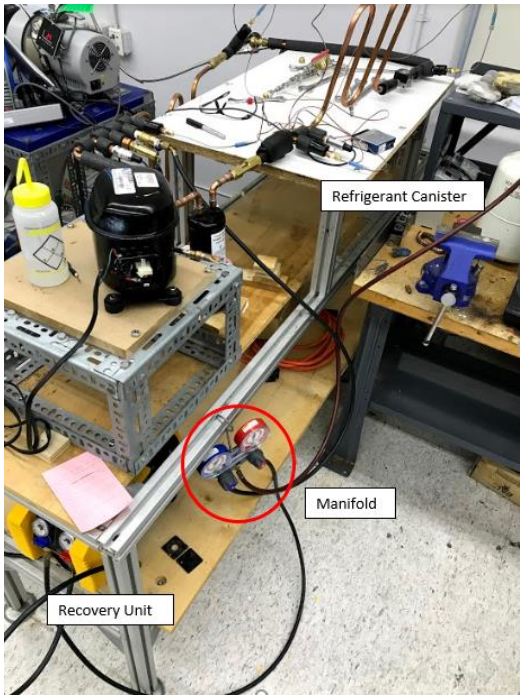

Figure 30: Cleaning setup

Although the VCC was designed to operate in ambient indoor conditions, as specified in the *Design* section, extra equipment was added to better simulate greenhouse conditions and ensure full phase change in both heat exchangers. Since the evaporator and condenser were sized based on ambient conditions, it is assumed that greater heat transfer will occur given the experimental setup, thus increasing the effectivity of the system and yielding better results. It was decided to use a commercial humidifier and aim it at the evaporator in order to better simulate humid greenhouse conditions. This will increase the amount of water condensed on the surface of the evaporator. In order to increase the heat rejected at the condenser, and therefore the rate of refrigerant condensation, the condenser was placed in an ice bath to provide a greater temperature differential. Although ecological adaptations will not mimic this setup, it will provide better results for our experiment by providing only liquid to the entrance of the evaporator. Furthermore, a fan was used over the evaporator to increase the rate of heat exchange from forced convection. A collection tray was used under the evaporator to weigh the total amount of condensed water during the tests. The experimental setup is shown in Figure 31 below.

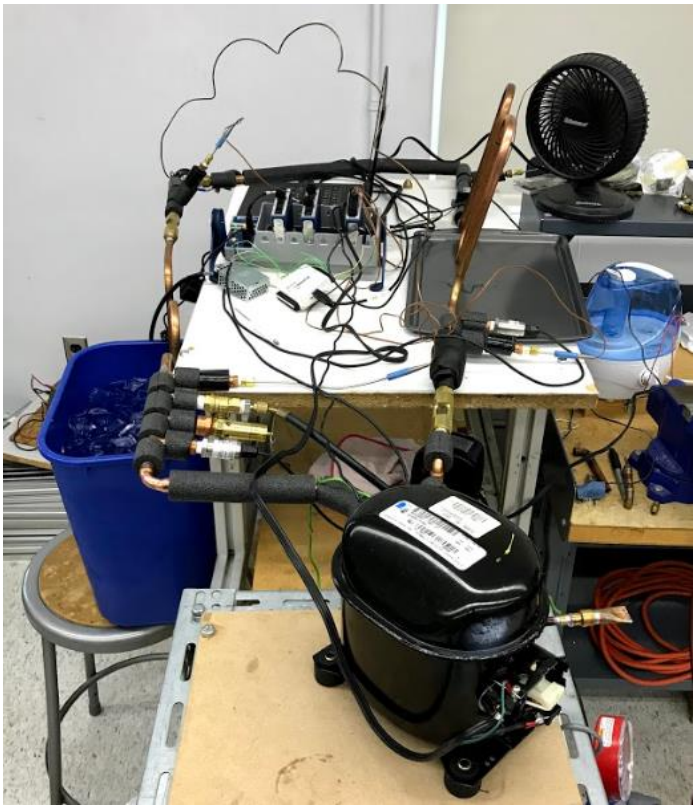

Figure 31: Final experimental setup

Experimental Results and Analysis

During the initial experimental run, about 77% of the calculated refrigerant weight (0.85 pounds) was added as a precautionary measure (see *Appendix 7* for weight calculation). The calculated value was determined by making several assumptions about the refrigerant phases throughout the cycle, and therefore is not indicative of the actual amount needed for optimal system performance. Since adding refrigerant to the system is quick and easy, a conservative amount was supplied at first to prevent any chance of over-pressurization. During this run, full refrigerant phase change occurred across the condenser, as verified by the temperature measurements and sight glass at the exit of the condenser. The significantly lower temperature exiting the condenser indicated that the refrigerant was not only condensing, but there was also significant sensible heat loss beyond the phase change. This occurred at pressures well below the calculated value of 780 kPa, due to the presence of ice water along the condenser. The operating pressures are shown in Figure 32 below.

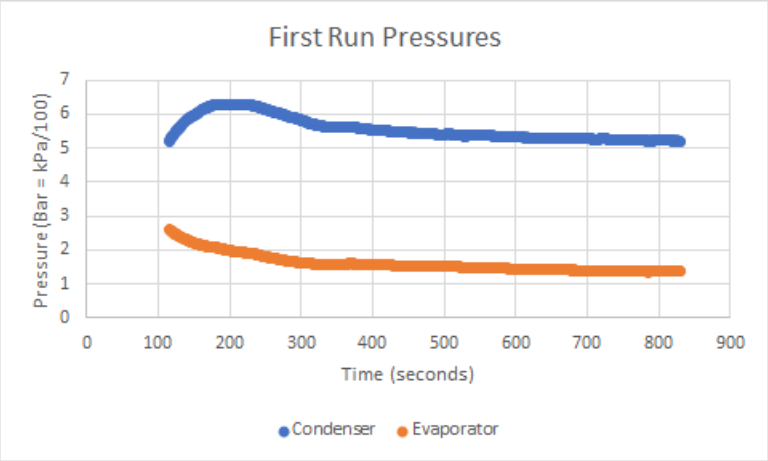

Figure 32: First run pressures

It was also verified that the compressor was providing adequate pressurization, as the outlet compressor temperature remained in the range of 41℃ to 49℃, just above our expected value of 41.5℃ as seen in Figure 33 below.

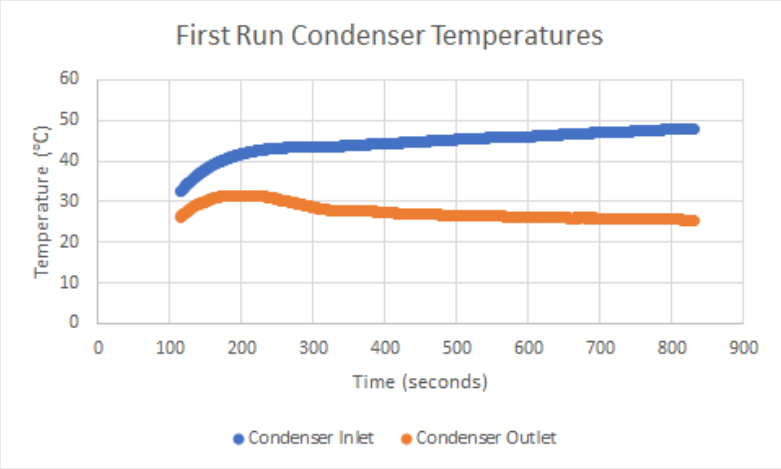

Figure 33: First run condenser temperatures

Since the ice bucket on the condenser provided excellent high-side performance, it was concluded after the first run that a large range of condensing pressures could be used and still provide satisfactory results. Although there was success with refrigerant condensation, the evaporator did not perform as expected. The low side pressure remained about 120 kPa, creating frost along the evaporator, as seen in Figure 34 below.

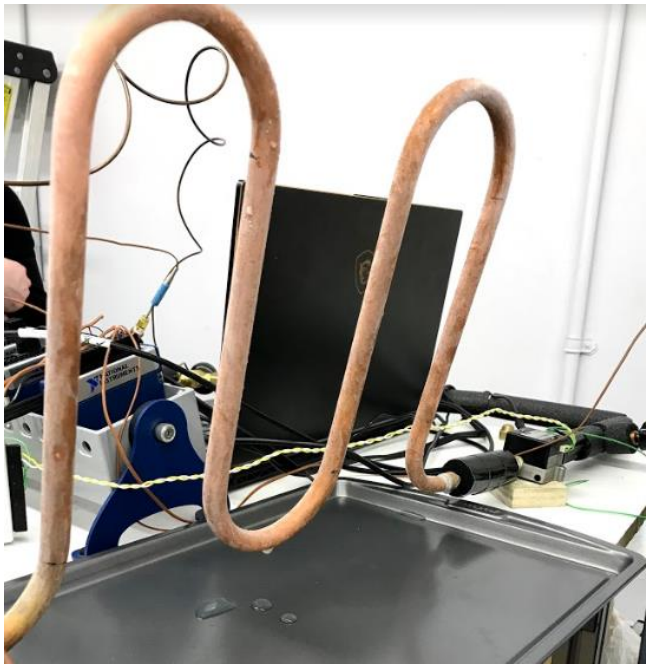

Figure 34: Frosted evaporator

Several problems were identified when trying to address the issue of frost formation on the evaporator. First, since the minimum flow rating on the expansion valve is higher than that experienced in the system, it could not raise the evaporator pressure to the calculated value of 179.4 kPa even when fully opened. Second, significant pressure drop between the two thermocouples on the evaporator side was experienced, causing the evaporator outlet temperature to be lower than the inlet, as seen from Figure 35 below.

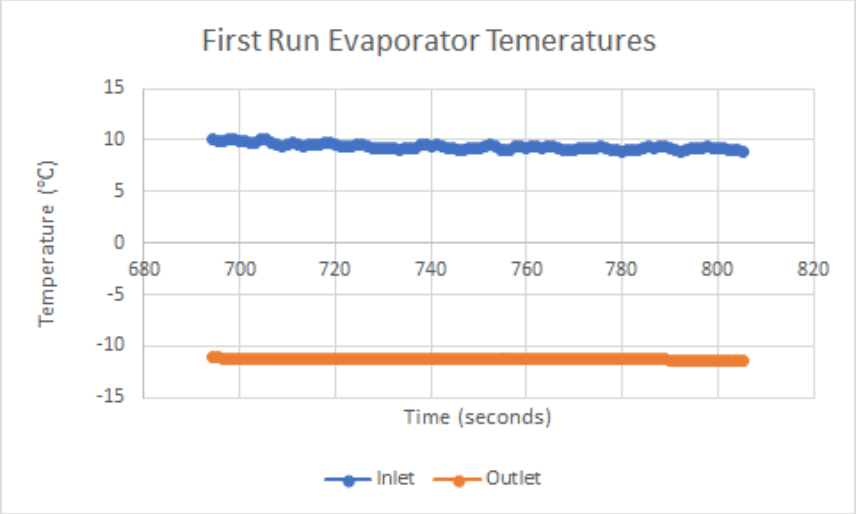

Figure 35: First run evaporator temperatures

The small inlet hole on the flow meter was hypothesized as the cause for this extreme pressure drop. Since incorrect flow readings were experienced during testing, probably due to too small of a flow rate or the flow meter being broken when the system was pressurized with compressed air during leak testing, the flow meter was removed and replaced with a precision valve, as seen in Figure 36 below.

Figure 36: Added precision valve

The precision valve functions to alleviate the pressure loss experienced with the flow meter, but also allow for precise control of the evaporator pressure, since the expansion valve was not functioning as intended. The precision valve proved to be effective in both of these aspects after a second run was done. By opening and closing the valve, the evaporator pressure throttled almost immediately, providing a controlled evaporator surface temperature slightly above freezing to prevent frost formation that occured in the first run. Instead, a layer of condensed water formed on the evaporator, providing a constant drip onto the collection tray, shown in Figure 37 below.

Figure 37: Evaporator with layer of condensed water

The exaggerated drop in pressure was also alleviated with the precision valve. The outlet of the evaporator still remained at a lower temperature due to slight pressure losses through the tube bends and

changing diameter through the precision valve, but the magnitude was much smaller than that experienced with the flow meter. The new evaporator inlet and outlet temperatures can be seen in Figure 38 below.

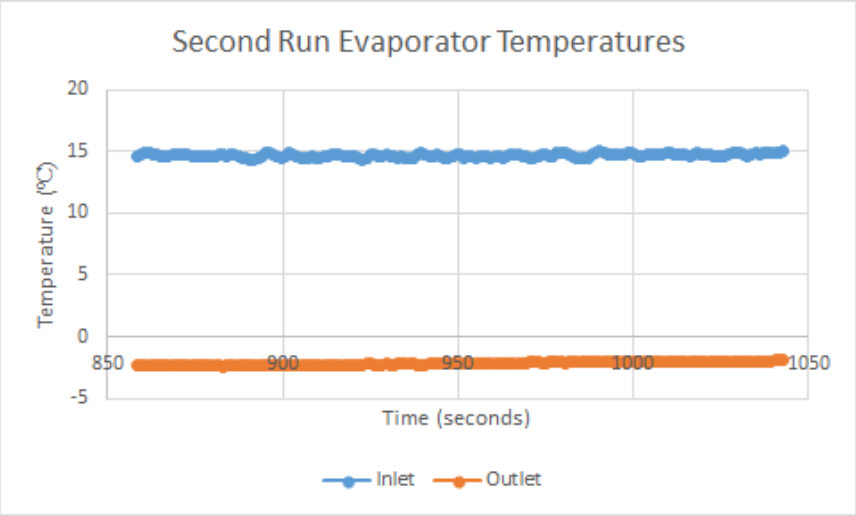

Figure 38: Second run evaporator temperatures

It was found that frost began to form when the refrigerant temperature reached around -3°C, so the precision valve was set so that the refrigerant temperature remained at about -1°C to -2°C. For this reason, the actual operating pressure had to be raised slightly above the calculated value to around 200 kPa (2 bar). Furthermore, since the condenser was placed in a bucket of ice water, the condenser pressure could take on a wide range of values while still providing full phase change. The ice water creates convective resistance values much higher than that of ambient air, which was not accounted for in the calculations. Consequently, at an operating pressure of around 700 kPa (7 bar), the refrigerant went through full phase change, as well as additional sensible heat loss. This can be seen from the inlet and outlet condenser temperature shown in Figure 39 below and the evaporator and condenser pressure in Figure 40.

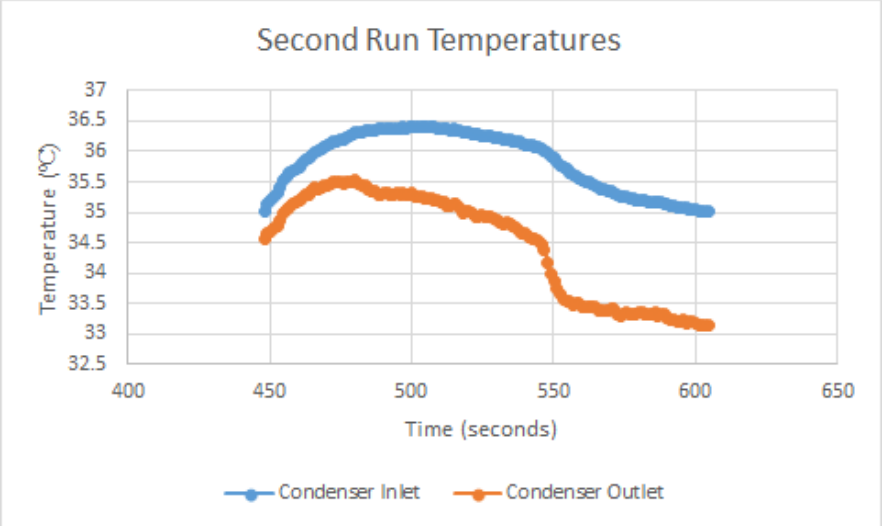

Figure 39: Second run condenser temperatures

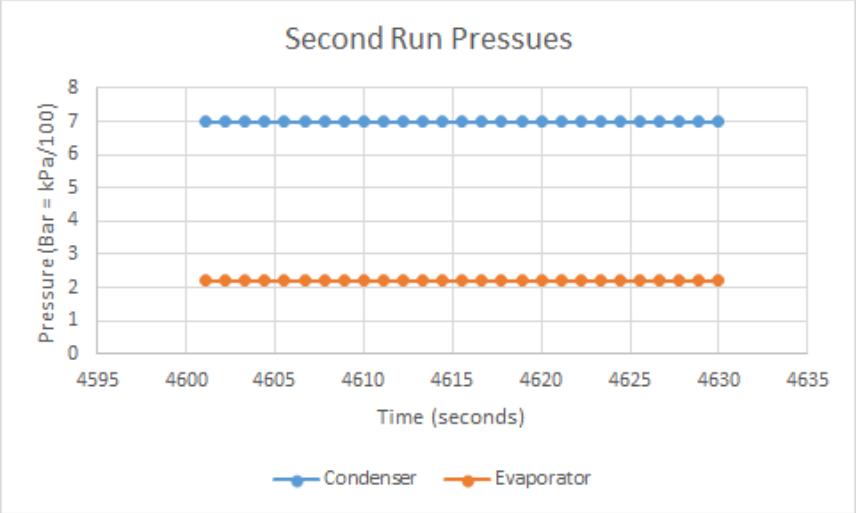

Figure 40: Second run pressures

The operating parameters achieved in the second run were close to those calculated in the *Design* section. The high and low side pressures were -10.3% and +10.0% off from the calculated values, respectively. The operating temperatures had a larger margin of error, however. The condenser and evaporator temperatures were -12.0% and -40% off from the calculated values, respectively. These deviations from the calculated values are a resultant of the improperly sized expansion valve, frost formation at a refrigerant temperature of -5°C, and the ice bucket that the condenser was placed in.

As previously mentioned, the flow meter that was purchased for the system was not functioning properly, so the refrigerant mass flow rate could not be verified. As a result, the heat transfer rate for both heat exchangers, and therefore the system COP, could not be determined and compared to the calculated values.

The amount of water generated in an hour was about 25cc. This was much lower than the specified goal of 500 cc/hr. This is because the goal value was somewhat arbitrary. The system was first simulated to produce 50cc/hour, however this resulted in small Q values for both heat exchangers and compressor work on the order of tens of watts. The rate of water condensation was then raised in order to raise the rate of heat exchange and compressor work to realistic values that would fit into a larger tabletop device. 500 cc/hour was used as a basis for the system values, with the presumption that the actual rate of condensation would be lower than 500 cc/hour. The actual rate of water collection was also low due to the small amount of evaporator surface area that came into contact with the humidifier stream. Since the evaporator turns were large, there was a lot of space between the vertical tubing for the humidifier stream to pass through. Had a coiled or flat plate heat exchanger been used, significantly more water would have been collected. The calculated rate of condensation per evaporator surface area was 11cc/(min.m^2). Had a square meter flat plate heat exchanger been used with the system operating parameters, 660 cc/hour of water would have been collected. This configuration would have also solved the issue of water layer formation on the evaporator surface, further improving the collection rate. Once the system reached steady state values, water quickly collected on the evaporator surface, however most of it remained there for the duration of the experiment. This thin water layer acts as a thermal barrier between the ambient air and the evaporator surface, so less water condenses. A means to remove that water, such as a hydrophobic

coating, flat plate heat exchanger, or a low frequency vibration would greatly increase the rate of water collection by allowing new water to form on the surface and immediately collect.

Cost Analysis

The following tables displays a cost break down of both the high and low sections of the fabricated VCC including the structure, instrumentation, equipment, insulation, valves, and fittings:

High Side & General Use Items:

Part Name	***Qty/Length***	***Cost/Unit***	***Cost Total***
Tecumseh Compressor	1 unit	$259.99	$259.99
Pressure Transmitter	1 unit	$115.36	$115.36
Thermostatic Expansion Valve	1 unit	$129.30	$129.30
⅜” Copper Tubing (Type L)	128.45 inches	$.0825/inch	$10.60
¼” Copper Tubing (Type L)	16.75 inches	$.1154/inch	$1.93
Air Safety Valve	1 unit	$38.23	$38.23
R1234ze Refrigerant	10 lbs	$305/10lbs	$305.00
Brazing Alloy	1 unit	$15.85	$15.85
Brazing Flux	1 unit	$25.08	$25.08
Copper Fittings	20 units	$4.54/unit	$90.80
Pipe Insulation	128.45 inches	$.0351/inch	$4.51
Thermocouple	2 units	$49.90	$99.80
Sight Glass	1 unit	$25.56/unit	$25.56
Binary Valve	1 unit	$11.71/unit	$11.71
Humidifier	1 unit	$36.31	$36.31
Total Cost			**$1,170.03**

Table 8: High side and general use costs

Low Side:

Part Name	*Qty/Length*	*Cost/Unit*	*Cost Total*
McMillan Flow Meter	1 unit	$683.36	$683.36
Pressure Transmitter	1 unit	$115.36	$115.36
Suction Line Accumulator	1 unit	$73.13	$73.13
⅜” Copper Tubing (Type L)	98.95 inches	$.0825/inch	$8.16
¼” Copper Tubing (Type L)	3.00 inches	$.1154/inch	$.35
Copper Fittings	18	$4.54/unit	$81.72
Pipe Insulation	98.95 inches	$.0351/inch	$3.47
Thermocouple	2 units	$49.90	$99.80
Sight Glass	1 unit	$25.56/unit	$25.56
Binary Valve	1 unit	$11.71/unit	$11.71
Total Cost			**$1,102.62**

Table 9: Low side costs

Final Cost Total:

Section	*Cost*
High Side & General Use Items	**$1,170.03**
Low Side	**$1,102.62**
Total Cost	**$2,272.65**

Table 10: Total system cost

In order to reduce cost on both sections of the system one could size the mating components such that the use of copper fittings (joints, tees, and couplings) is minimized. Due to time constraints and size constraints of our instruments and components, this was not a priority in procurement. Further, given the limited tooling and molding ability, a large amount of copper piping (and therefore insulation) was used to join the bent sections of the system, as such, cost could be minimized here by creating tighter angles and more acute bends in the piping. One of the most critical components in this system is the Suction Line Accumulator, which disallows liquid from entering the compressor, which is a fatal flaw. The

Suction Line Accumulator is effectively an insurance policy for the costly compressor shown in the High Side & General Use Items table above.

Conclusions & Recommendations

The vapor compression cycle was shown to be effective in condensing and collecting atmospheric water vapor and served as an effective proof of concept. Although the specified goal of 500cc/hour was not achieved due to the evaporator geometry and improperly sized equipment, a high rate of condensation per surface area was experienced, providing promising results for future experiments. At a rate of 11 $cc/(min.m^2)$, a system with the same operating parameters and more favorable evaporator geometry would be able to generate well over 500 cc/hour, and would be extremely efficacious when incorporated into a large scale system. Future work, involving the use of coiled or flat plate evaporators, enhanced surfaces on both heat exchangers, and EHD pumping in both heat exchangers is necessary to improve system performance and optimize the rate of water collection. Furthermore, the evaporator refrigeration tonnage needs to be increased in order for proper functioning of the expansion valve and a larger refrigerant mass flow rate is necessary for accurate flow meter output to verify the rate of heat transfer and system COP. Though testing in actual greenhouse conditions is necessary to verify the applicability of VCC in large scale ecological systems, this project demonstrates that atmospheric water generation using VCC is achievable.

References

American Society of Heating, Refrigerating and Air Conditioning Engineers. (1994). ASHRAE 15: Safety Code for Mechanical Refrigeration. Atlanta, GA: Author. Retrieved from https://archive.org/details/gov.law.ashrae.15.1994/page/n11

Atta, Raghied. (2011). *Solar Water Condensation Using Thermoelectric Coolers*. Retreived from https://www.researchgate.net/publication/267700639_Solar_Water_Condensation_Using_Thermoelectric_Coolers

Chandler, D. (2017). Water, water everywhere … even in the air. Retrieved from http://news.mit.edu/2017/MOF-device-harvests-fresh-water-from-air-0414

D. Milani. (2012). *Modelling framework of solar assisted dehumidification system to generate freshwater from "Thin air"* (Doctoral dissertation). Retrieved from https://www.researchgate.net/publication/280082882/download

Desiccants: Technical Data and Terminology. (n.d.) Retreived from https://www.sorbentsystems.com/desiccants_terminology.html

Furukawa, H., Cordova, K., O'Keeffe, M., & Yaghi, O. (2013). The Chemistry and Applications of Metal-Organic Frameworks. Science Magazine, (341), 974.

Honeywell Refrigerants. (2017). *Solstice® ze Refrigerant: Safety Data Sheet*. Heverlee, Belgium: Author

Illsley, C. (2016, March 21). *Top Bottled Water Consuming Countries*. Retrieved from https://www.worldatlas.com/articles/top-bottled-water-consuming-countries.html

Kirkpatrick, A. (2017). *Introduction to refrigeration and air conditioning systems: theory and applications*. Retrieved from https://ebookcentral-proquest-com.ezproxy.wpi.edu

Muller, C., & Scholz, D. (2004).*The Vapor Compression Cycle in Aircraft Air-Conditioning Systems*. Retrieved from http://www.fzt.haw-hamburg.de/pers/Scholz/FLECS/FLECS_TN_Vapor-Cycle_17-01-04.pdf

National Society of Professional Engineers. (2018). *NSPE Code of Ethics for Engineers*. Alexandria, VA: Author. Retrieved from https://www.nspe.org/resources/ethics/code-ethics

Service, R. (2017). This new solar-powered device can pull water straight from the desert air. Retrieved from https://www.sciencemag.org/news/2017/04/new-solar-powered-device-can-pull-water-straight-desert-air

The Ideal Vapor Compression Refrigeration Cycle (2018). Retrieved from http://slideplayer.com/slide/1424579/4/images/9/THE+IDEAL+VAPOR-COMPRESSION+REFRIGERATION+CYCLE.jpg

Thermoacoustic refrigeration. (n.d.) Retrieved from http://www.grimsby.ac.uk/documents/defra/tech-thermoacoustic.pdf

Water Crisis - Learn About The Global Water Crisis. (n.d.). Retrieved from https://water.org/our-impact/water-crisis/

Water Desalination Processes. (n.d.). Retrieved from https://www.amtaorg.com/Water_Desalination_Processes.html

Welch, Terry. (2008). *Refrigeration - CIBSE Knowledge Series: KS13 - 5. How the Vapour Compression Cycle Works.* CIBSE. Retrieved from https://app.knovel.com/hotlink/pdf/id:kt00U1B9I4/refrigeration-cibse-knowledge/how-vapour-compression

World Water Treatment Equipment. (n.d.). Retrieved from https://www.freedoniagroup.com/industry-study/world-water-treatment-equipment-3103.htm

Zhao, L., Cai, W., Ding, X., & Chang, W. (2013). *Decentralized optimization for vapor compression refrigeration cycle*. Applied Thermal Engineering, 51(1-2), 753-763. doi: 10.1016/j.applthermaleng.2012.10.001

Appendix 1: R-1234ze Pressure-Enthalpy Data

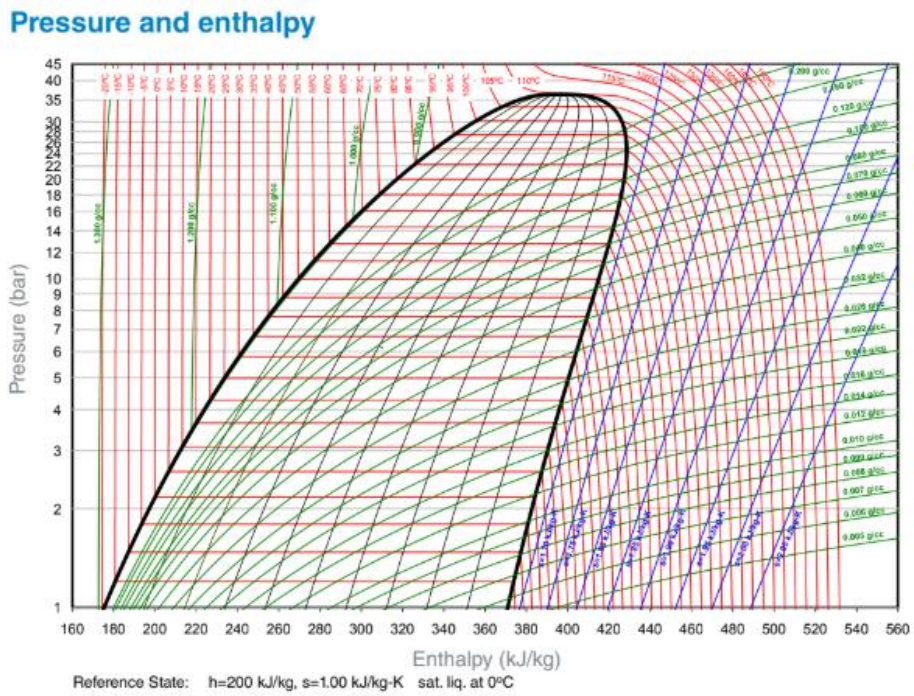

Figure 41: R-1234ze pressure-enthalpy data

Appendix 2: R-1234ze Pressure-Temperature Data

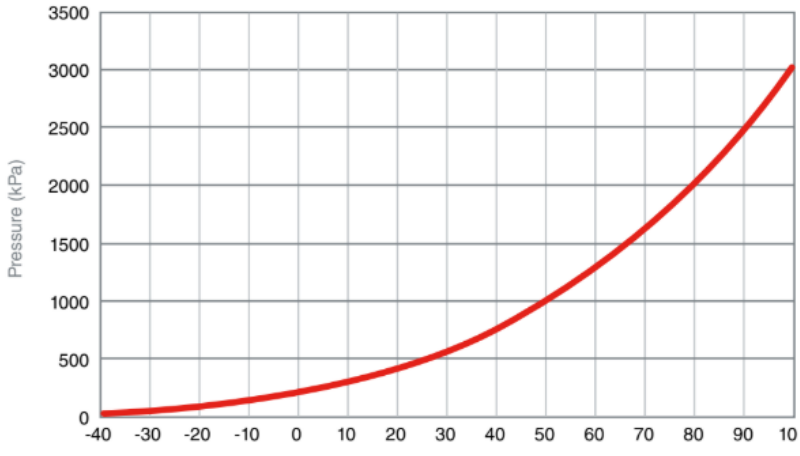

$$\log_{10}(\text{Press}) = \frac{A_0}{T + 273.15 + A_1} + A_2$$

with $A_0 = -1115.58$ (bar, °C)

$A_1 = -6.78$

$A_2 = 4.52$

Figure 42: R-1234ze pressure-temperature data

Appendix 3: R-134a Comparison

Comparison 134a alternatives

	134a	1234ze
ASHRAE class	A1	A2L
GWP (rev 5th IPCC)	1300	<1
LFL (vol% in air)*	N/A	7% **
UFL (vol% in air)*	N/A	12% **
Heat of Combustion (kJ/g)	4.2	10.7
Burning Velocity (cm/s)	N/A	N/A
Minimum Ignition Energy (mJ)	N/A	61000 to 64000 ***
PED (97/23/EC) class	2	2
Flammability for handling and storage	No	No
Commercial availability	Yes	Yes
Ease of adoption	Baseline	Moderate – Easy when systems can be designed
Cost of adoption	Baseline	Moderate

*Flame limits- ASTM E681-04 at 21°C; **(at 100°C); ***(at 54°C)

Figure 43: R-134a comparison

Appendix 4: Evaporator Length Script

```
% Evaporator
Re = ((4*m_dot)/(pi*Di*mu_l)); %kg/s, m, Pa-s
Q = Qin/(pi*(Do^2));
Re_v = ((4*m_dot)/(pi*Di*mu_v)); %(Q*Lg)/(hfg*mu_v)
h = (k_l/Di)*(1.3+(39*Di))*((Pr^0.9)*(Re^0.23)*(Re_v^0.34)*((p_l/p_v)^0.25)*(mu_v/mu_l));
UA_e = Qin/10;
syms L
eqn1 =  (1/UA_e) - ((1/(h*pi*Di*L)) + (((log(Do/Di))/(2*pi*385*L)))) == 0;
sol = solve(eqn1,L);
```

Figure 44: Evaporator length Matlab script

Appendix 5: Condenser Length Script

```
%Condenser
P2 = 780;
T2 = 31.04*log(P2) - 166.51;
k = (((2*10^-5)*P2^2- .0496*P2 +93.193)*10^-3); %.0689
p_l = (0.0001*P2^2 - 0.3879*P2 + 1320.3); %1110
p_v = (0.0531*P2 + 0.0458); %41.38
mu_l = ((-82.55*log(P2) + 714.37)*10^-6); %165.72*10^-6
mu_v = (((-2*10^-06)*P2^2 + 0.0053*P2 + 10.095)*10^-6); %12.96*10^-6;
Pr_l = 3.47;
Re_v = (4*m_dot)/(pi*Di*mu_v);
Re_l = (4*m_dot)/(pi*Di*mu_l);
Re_tp = (Re_v*((p_l/p_v)^0.5)*(mu_v/mu_l)) + Re_l;
hi = (k/Di)*(0.05*(Re_tp^0.8))*(Pr_l^0.33);
Wc = (m_dot*.008314*(273+T1)*3.5*((P2/P1)^(.4/1.4)-1))/0.6;
UA_c = (Qin + (Wc*1000))/20
syms L_c
eqn1 =  (1/UA_c) - ((1/(hi*pi*Di*L_c)) + ((log(Do/Di))/(2*pi*385*L_c))) == 0;
sol = solve(eqn1,L_c);
```

Figure 45: Condenser length Matlab script

Appendix 6: Detailed P&ID

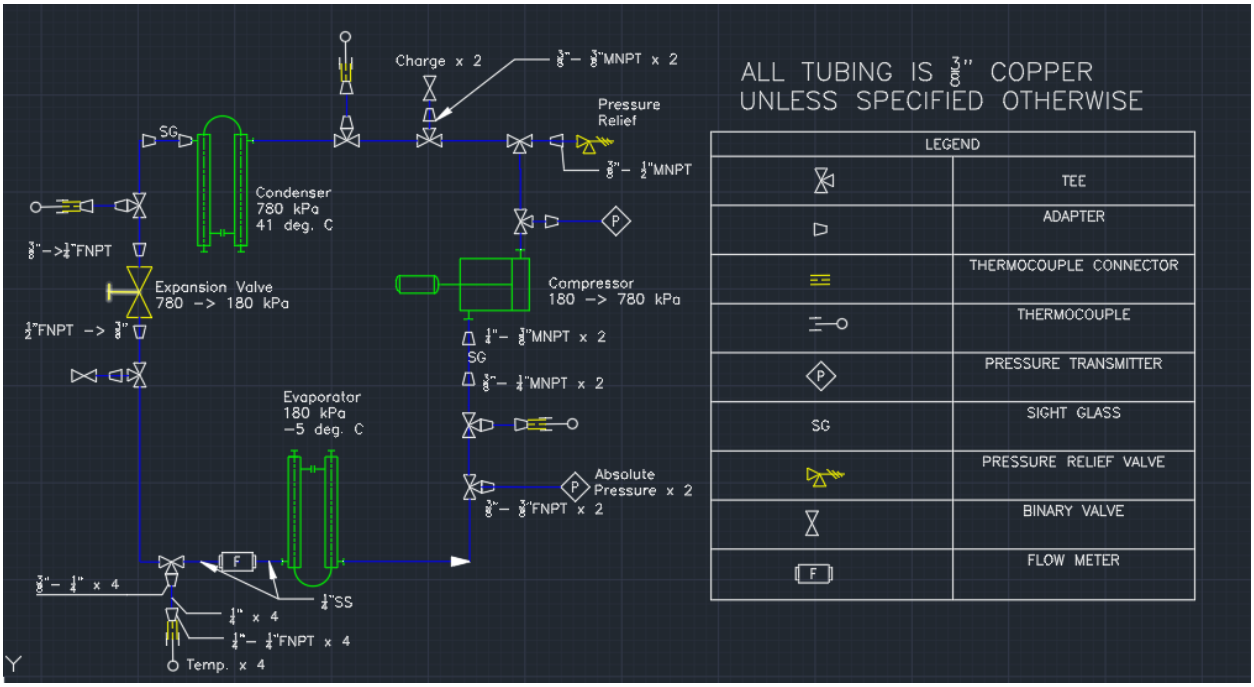

Figure 46: Detailed P&ID

Appendix 7: Refrigerant Weight Calculations

ID	0.41	0.16	
R	0.205	0.08	
Area	0.1320254313	0.02010619298	
Liquid Length	128.45	16.75	
Vapor Length	98.95	3	
Liquid Volume	16.95866665	0.3367787325	
Vapor Volume	13.06391642	0.06031857895	
Liquid Density	0.0467	0.0467	
Vapor Density	0.0002	0.0002	
Weight	0.7945825157	0.01573963052	0.8103221462
SLA	0.00856531049		
Hose	0.2750857067		
Total	1.093973163		

Table 11: Refrigerant weight calculations

Appendix 8: LabView Front Panel

Figure 47: LabView front panel

Appendix 9: LabView Block Diagram

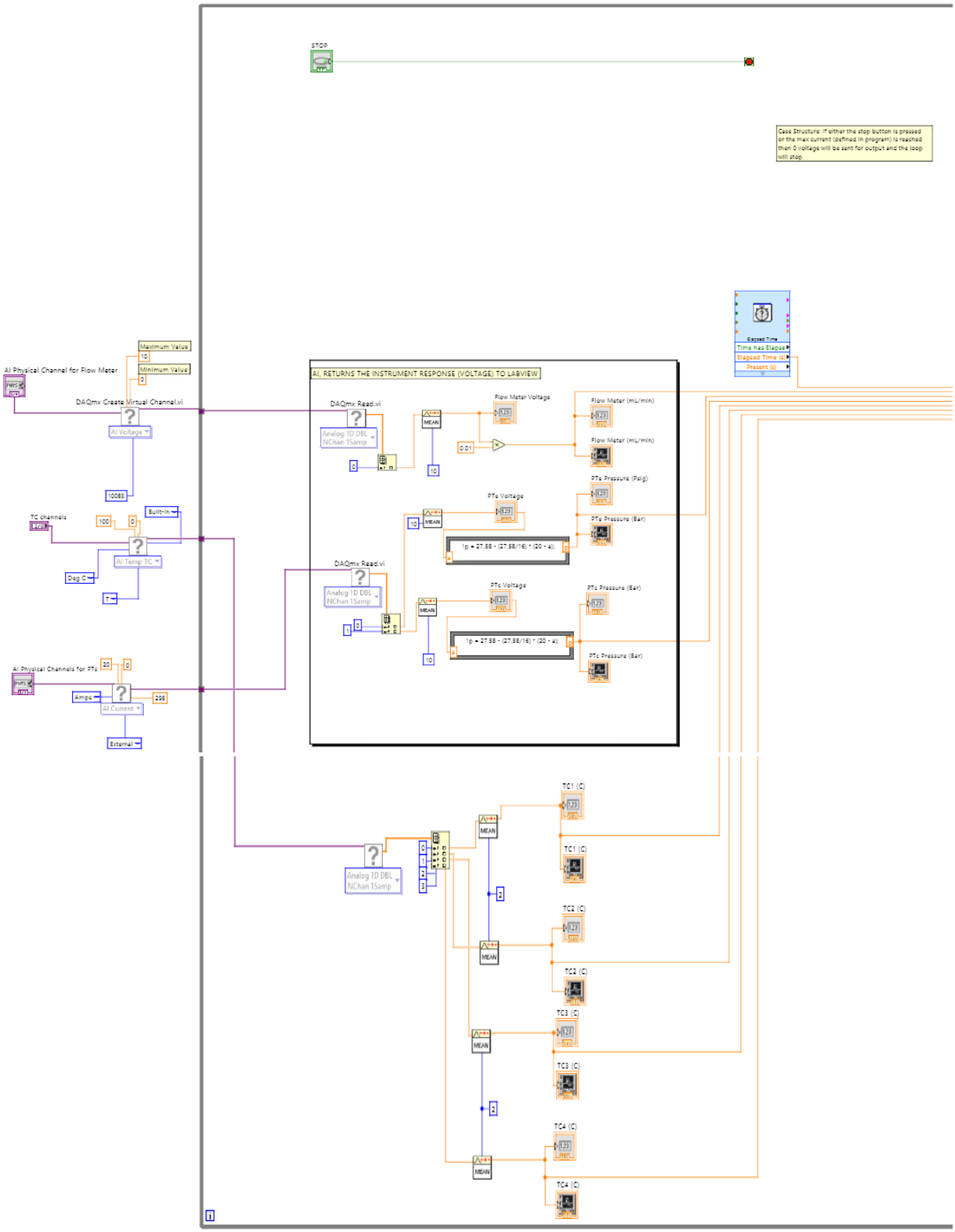

Figure 48: Left side of block diagram

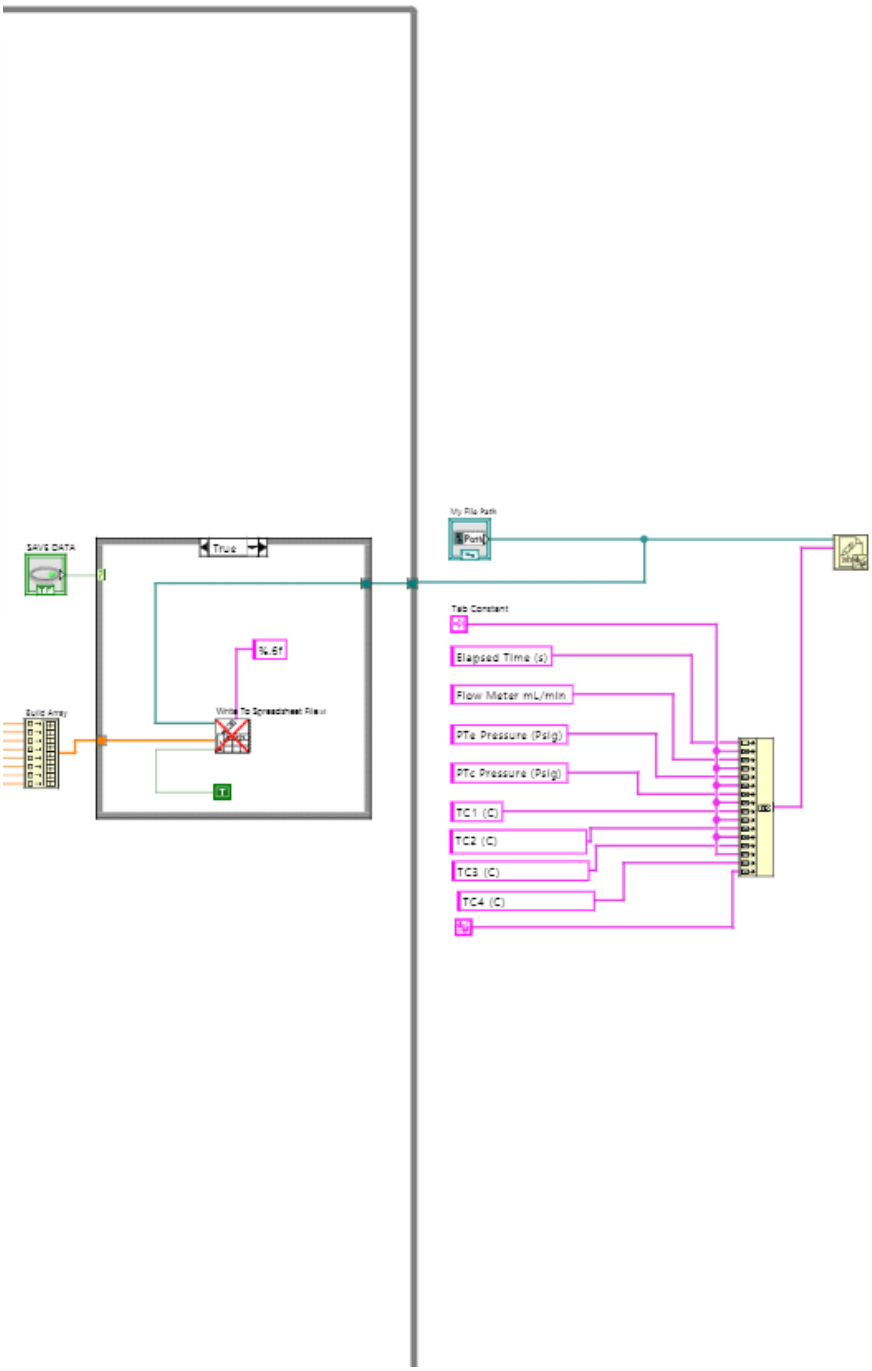

Figure 49: Right side of block diagram